

## RESEARCH ARTICLE

## INFECTION

# Hyperglycemia drives intestinal barrier dysfunction and risk for enteric infection

Christoph A. Thaiss,<sup>1</sup> Maayan Levy,<sup>1</sup> Inna Grosheva,<sup>2</sup> Danping Zheng,<sup>1</sup> Eliran Soffer,<sup>1</sup> Eran Blacher,<sup>1</sup> Sofia Braverman,<sup>1</sup> Anouk C. Tengeler,<sup>1</sup> Oren Barak,<sup>1,3</sup> Maya Elazar,<sup>1</sup> Rotem Ben-Zeev,<sup>1</sup> Dana Lehavi-Regev,<sup>1</sup> Meirav N. Katz,<sup>1</sup> Meirav Pevsner-Fischer,<sup>1</sup> Arieh Gertler,<sup>4</sup> Zamir Halpern,<sup>5,6,7</sup> Alon Harmelin,<sup>8</sup> Suhail Aamar,<sup>9</sup> Patricia Serradas,<sup>10</sup> Alexandra Grosfeld,<sup>10</sup> Hagit Shapiro,<sup>1</sup> Benjamin Geiger,<sup>2</sup> Eran Elinav<sup>1\*</sup>

Obesity, diabetes, and related manifestations are associated with an enhanced, but poorly understood, risk for mucosal infection and systemic inflammation. Here, we show in mouse models of obesity and diabetes that hyperglycemia drives intestinal barrier permeability, through GLUT2-dependent transcriptional reprogramming of intestinal epithelial cells and alteration of tight and adherence junction integrity. Consequently, hyperglycemia-mediated barrier disruption leads to systemic influx of microbial products and enhanced dissemination of enteric infection. Treatment of hyperglycemia, intestinal epithelial-specific GLUT2 deletion, or inhibition of glucose metabolism restores barrier function and bacterial containment. In humans, systemic influx of intestinal microbiome products correlates with individualized glycemic control, indicated by glycosylated hemoglobin levels. Together, our results mechanistically link hyperglycemia and intestinal barrier function with systemic infectious and inflammatory consequences of obesity and diabetes.

The obesity pandemic has reached alarming magnitudes, affecting more than 2 billion people worldwide and accounting for more than 3 million deaths per year (1). A poorly understood feature of the “metabolic syndrome” is its association with dysfunctions of the intestinal barrier, leading to enhanced permeability and translocation of microbial molecules to the intestinal lamina propria and systemic circulation (2). This influx of immune-stimulatory microbial ligands into the vasculature, in turn, has been suggested to underlie the chronic inflammatory processes that are frequently observed in obesity and its complications (3), while entry of pathogens and pathobionts through an impaired barrier leads to an enhanced risk of infection in obese and diabetic individuals (4, 5), particularly

at mucosal sites (6). However, the mechanistic basis for barrier dysfunction accompanying the metabolic syndrome remains poorly understood. Beyond metabolic disease, enhanced intestinal permeability has also been linked with systemic inflammation in a variety of conditions, including cancer (7), neurodegeneration (8), and aging (9). Thus, there is an urgent scientific need to better define the molecular and cellular orchestrators and disruptors of intestinal barrier function, to devise strategies to counteract the detrimental systemic consequences of gut barrier alterations.

## Obesity is associated with, but not required for, intestinal barrier dysfunction

We began our investigation of the drivers of gastrointestinal barrier dysfunction in obesity by hypothesizing that the adipokine leptin, a major orchestrator of mammalian satiety, may act as an obesity-associated regulator of barrier integrity. Leptin deficiency and resistance to leptin signaling are strongly associated with morbid obesity in mice and humans, and both leptin deficiency and resistance were previously suggested to contribute to intestinal barrier dysfunction and susceptibility to enteric infection (10–13). We used a mouse model featuring genetic dysfunction of the leptin receptor (LepR), leading to hyperphagia and morbid obesity (*db/db*, fig. S1A). Indeed, we detected elevated amounts of microbial pattern recognition receptor (PRR) ligands at multiple systemic sites in leptin-

unresponsive *db/db* mice (Fig. 1, A to C), indicative of enhanced influx of gut commensal-derived products. A similar phenomenon was observed in leptin-deficient mice (*ob/ob*, fig. S1, B and C). To gain insight into the molecular signatures accompanying barrier dysfunction under aberrant leptin signaling, we performed RNA sequencing of colonic tissue, obtained from *db/db* mice and their wild-type (WT) littermates under steady-state conditions. Leptin unresponsiveness was associated with global alterations of transcription (fig. S1D), with several hundred genes featuring differential expression between both groups (fig. S1E). Among the genes whose expression was most strongly abrogated in obese mice were members of the tight and adherence junction structures (fig. S1F), protein complexes that inhibit paracellular flux of intestinal molecules into the lamina propria (14). Consequently, tight junction integrity was compromised in *db/db* mice (Fig. 1, D and E), leading to enhanced influx of luminal molecules and electrical current measured across the epithelial layer (Fig. 1, F and G).

To determine the consequences of barrier dysfunction in leptin-resistant mice, we used the murine *Citrobacter rodentium* model simulating human enteropathogenic *Escherichia coli* infection (15). A bioluminescent variant of *C. rodentium* allowed us to noninvasively track infection in vivo (16). In WT mice, *C. rodentium* caused a self-limiting, mainly gut-contained infection (Fig. 1, H to L). In contrast, *db/db* mice did not clear the pathogen from their intestine (Fig. 1, H and I), in line with previous reports (12). Notably, *db/db* mice also showed a significantly enhanced bacterial attachment to the intestinal wall (fig. S1, G and H) and featured *C. rodentium* colonization at systemic sites (Fig. 1, J to L, and fig. S1I). Similar susceptibility to *C. rodentium* was noted for leptin-deficient *ob/ob* mice (fig. S1, J to N).

To understand which cell type was responsible for LepR-mediated protection from enteric infection, we generated bone marrow chimeras, in which WT and *db/db* mice were used as either recipients or donors of bone marrow transplanted into lethally irradiated mice. Exacerbated infection and systemic spread of *C. rodentium* was observed whenever the bone marrow recipient was LepR-deficient, regardless of the source of bone marrow (Fig. 1, M and N, and fig. S1O), indicating that the nonhematopoietic compartment mediated resistance against infection. LepR expression on nonhematopoietic cells has been reported in multiple tissues, including the gut, liver, and most prominently the nervous system (17). Mice lacking LepR in intestinal epithelial cells (Villin-Cre:LepR<sup>fl/fl</sup>) or hepatocytes (Albumin-Cre:LepR<sup>fl/fl</sup>) did not show any signs of enhanced susceptibility to *C. rodentium* infection (fig. S2, A to F), whereas mice with LepR deficiency specifically in the nervous system (Nestin-Cre:LepR<sup>fl/fl</sup>) featured an exacerbated (fig. S2, G to I), yet highly variable (fig. S2, J to O), bacterial growth. To further explore the possibility of neuronal leptin signaling driving barrier dysfunction and risk of infection, we generated mice with a specific

<sup>1</sup>Department of Immunology, Weizmann Institute of Science, Rehovot, Israel. <sup>2</sup>Department of Molecular Cell Biology, Weizmann Institute of Science, Rehovot, Israel. <sup>3</sup>Department of Obstetrics and Gynecology, Kaplan Medical Center, Rehovot, affiliated with the Hebrew University and Hadassah School of Medicine, Jerusalem, Israel. <sup>4</sup>The Robert H. Smith Faculty of Agriculture, Food and Environment, The Hebrew University, Rehovot, Israel. <sup>5</sup>Sackler Faculty of Medicine, Tel Aviv Sourasky Medical Center, Tel Aviv, Israel. <sup>6</sup>Research Center for Digestive Tract and Liver Diseases, Tel Aviv Sourasky Medical Center, Tel Aviv, Israel. <sup>7</sup>Digestive Center, Tel Aviv Sourasky Medical Center, Tel Aviv, Israel. <sup>8</sup>Department of Veterinary Resources, Weizmann Institute of Science, Rehovot, Israel. <sup>9</sup>Department of Medicine, Hadassah-Hebrew University Hospital, Jerusalem, Israel. <sup>10</sup>INSERM Centre de Recherche des Cordeliers, Sorbonne Université, Sorbonne Cité, UPD Univ. Paris 05, CNRS, IHU ICAH, Paris, France.

\*Corresponding author. Email: eran.elinav@weizmann.ac.il

deletion of LepR in the paraventricular hypothalamus (Sim1-Cre:LepR<sup>fl/fl</sup>), in the ventromedial hypothalamus (SF1-Cre:LepR<sup>fl/fl</sup>), in cholinergic neurons (ChAT-Cre:LepR<sup>fl/fl</sup>), and in the arcuate nucleus of the hypothalamus (POMC-Cre:LepR<sup>fl/fl</sup> and AgRP-Cre:LepR<sup>fl/fl</sup>) and infected them with *C. rodentium*. However, none of these mice showed enhanced susceptibility to pathogenic invasion when compared to littermate controls (fig. S3, A to O). Collectively, these results suggested that leptin deficiency per se might not provide a sufficient explanation to barrier dysfunction and enhanced risk of enteric infection.

A feature common to all leptin- and LepR-deficient mice exhibiting an impaired barrier function and enhanced *C. rodentium* dissemination in our studies (*db/db*, *ob/ob* and Nestin-Cre:LepR<sup>fl/fl</sup>) was their tendency to develop obesity. We therefore hypothesized that an obesity-related factor distinct from leptin signaling may pre-

dispose these mice to impaired barrier function and exacerbated intestinal infection. Thus, to complement the above genetic models of obesity, we fed WT mice a high-fat diet (HFD) to induce weight gain (fig. S4A). Similarly to obese leptin- and LepR-deficient mice, HFD-fed obese mice showed elevated steady-state systemic PRR ligand and influx (Fig. 2A), as well as exacerbated *C. rodentium* infection and systemic dissemination (Fig. 2, B to E, and fig. S4B). To further test whether obesity is the major driver for barrier dysfunction and impaired *C. rodentium* containment in LepR-deficient mice, we performed paired-feeding experiments, in which the food access for *db/db* mice was restricted to the amount consumed by their WT littermates, thereby equalizing body weight between both groups (Fig. 2F). Surprisingly, even after weight reduction to control levels, lean *db/db* mice were still unable to cope with *C. rodentium* infection (Fig. 2, G and

H), ruling out that obesity per se was directly driving barrier dysfunction and risk for enteric infection in these mice. The lack of a direct causal relationship between obesity and barrier dysfunction was further supported by experiments using a chemical inhibitor of leptin signaling (18), which rendered WT mice susceptible to exacerbated infection and systemic bacterial spread even before the onset of marked obesity (Fig. 2, I to L, and fig. S4, C to F). Together, these data indicated that neither leptin signaling nor obesity per se sufficiently explain the severity of barrier dysfunction and systemic enteric infection in mice with the metabolic syndrome.

In search of a unifying explanation for the above results in multiple mouse models of genetic and acquired obesity and leptin deficiency, we investigated other common features of the metabolic syndrome that could potentially contribute to barrier dysfunction. One such manifestation

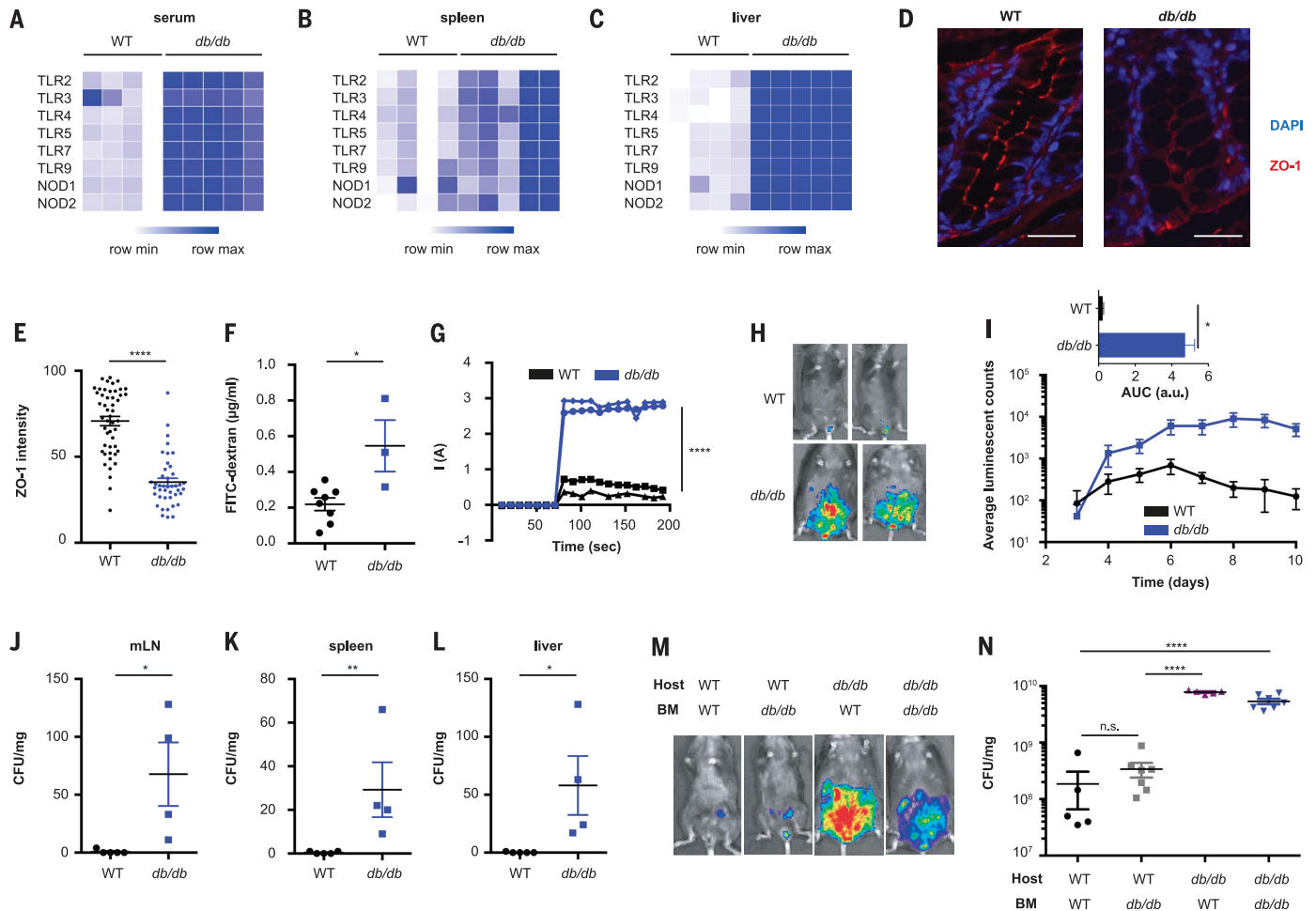


**Fig. 1. Obesity is associated with intestinal barrier dysfunction and enteric infection.** (A to C) PRR stimulation by sera (A) and splenic (B) and hepatic extracts (C) from *db/db* mice and WT littermates. (D and E) ZO-1 staining (D) and quantification (E) of colonic sections from *db/db* mice and WT littermates. Scale bars, 100 μm. (F) FITC (fluorescein isothiocyanate)-dextran recovered from the serum of *db/db* mice and WT littermates after oral gavage. (G) Ussing chamber recording of colons from *db/db* mice and controls. (H to L) Abdominal luminescence (H and I) and

colony-forming units (CFUs) recovered from mesenteric lymph nodes (J), spleens (K), and livers (L) from *db/db* mice infected with *C. rodentium*. (M and N) Total abdominal luminescence (M) and epithelial-adherent colonies (N) of *C. rodentium* in bone marrow chimeras of *db/db* and WT mice. All data represent at least two independent experiments. Means ± SEM are plotted. \* $P < 0.05$ , \*\* $P < 0.01$ , \*\*\*\* $P < 0.0001$  by analysis of variance (ANOVA) (N) or Mann-Whitney *U* test (all other panels). ns, not significant.

of the metabolic syndrome, typically accompanying obesity and potentially contributing to barrier dysfunction, is glucose intolerance and resultant hyperglycemia. Notably, all mice featuring marked susceptibility *C. rodentium* infection, including obese *db/db*, pair-fed lean *db/db* mice, Nestin-Cre: LepR<sup>fl/fl</sup> mice, mice fed a HFD, and mice treated with leptin antagonist, showed elevated blood glucose concentrations (Fig. 2, M to O, and fig. S4, G and H). In contrast, all mouse groups and models that did not develop enhanced *C. rodentium* susceptibility (Villin-Cre: LepR<sup>fl/fl</sup>, Albumin-Cre: LepR<sup>fl/fl</sup>, Sim1-Cre: LepR<sup>fl/fl</sup>, SFI-Cre: LepR<sup>fl/fl</sup>, ChAT-Cre: LepR<sup>fl/fl</sup>, POMC-Cre: LepR<sup>fl/fl</sup>, and AgRP-Cre: LepR<sup>fl/fl</sup>, as well as those Nestin-Cre: LepR<sup>fl/fl</sup> mice that did not feature a tendency for severe infection) collectively showed normoglycemic levels (fig. S4, I and J). Together, these results suggested that hyperglycemia, rather than obesity or alterations in leptin signaling, may predispose to barrier

dysfunction leading to enhanced enteric infection in the setup of the metabolic syndrome in mice.

### Hyperglycemia drives intestinal barrier disruption

To test whether elevated glucose concentrations were causally involved in host defense against intestinal infection, we induced hyperglycemia in the absence of obesity in a mouse model of type 1 diabetes mellitus through administration of streptozotocin [STZ (19), fig. S5A]. Indeed, STZ-treated mice developed severe *C. rodentium* infection and systemic translocation, accompanied by enhanced bacterial growth, epithelial adherence, and systemic spread (Fig. 3, A to E). STZ treatment also resulted in dysfunction of intestinal epithelial adherence junctions under steady-state conditions (Fig. 3, F and G), coupled with systemic dissemination of microbial products (fig. S5, B and C), and enhanced transepithelial flux (Fig. 3, H and I).

Oral antibiotic treatment prevented the detection of bacterial products at systemic sites in STZ-treated mice (Fig. 3, J to L), demonstrating that the intestinal microbiota was the probable source of disseminated microbial molecules. In contrast to the load of bacterial products at distal organs (fig. S5D), the microbial load in the intestinal lumen was unaffected by hyperglycemia (fig. S5E). We next sought to test the possibility that barrier dysfunction in STZ-treated mice was mediated by compositional microbiota alterations. Indeed, 16S ribosomal DNA (rDNA) sequencing revealed a taxonomic change in the configuration of the intestinal microbiota of hyperglycemic mice, which was corrected by insulin treatment and resultant normalization of serum glucose concentrations (fig. S6, A to D). However, these compositional microbial changes did not seem to play a critical role in glucose-mediated barrier dysfunction, as microbiota transfer from STZ-treated

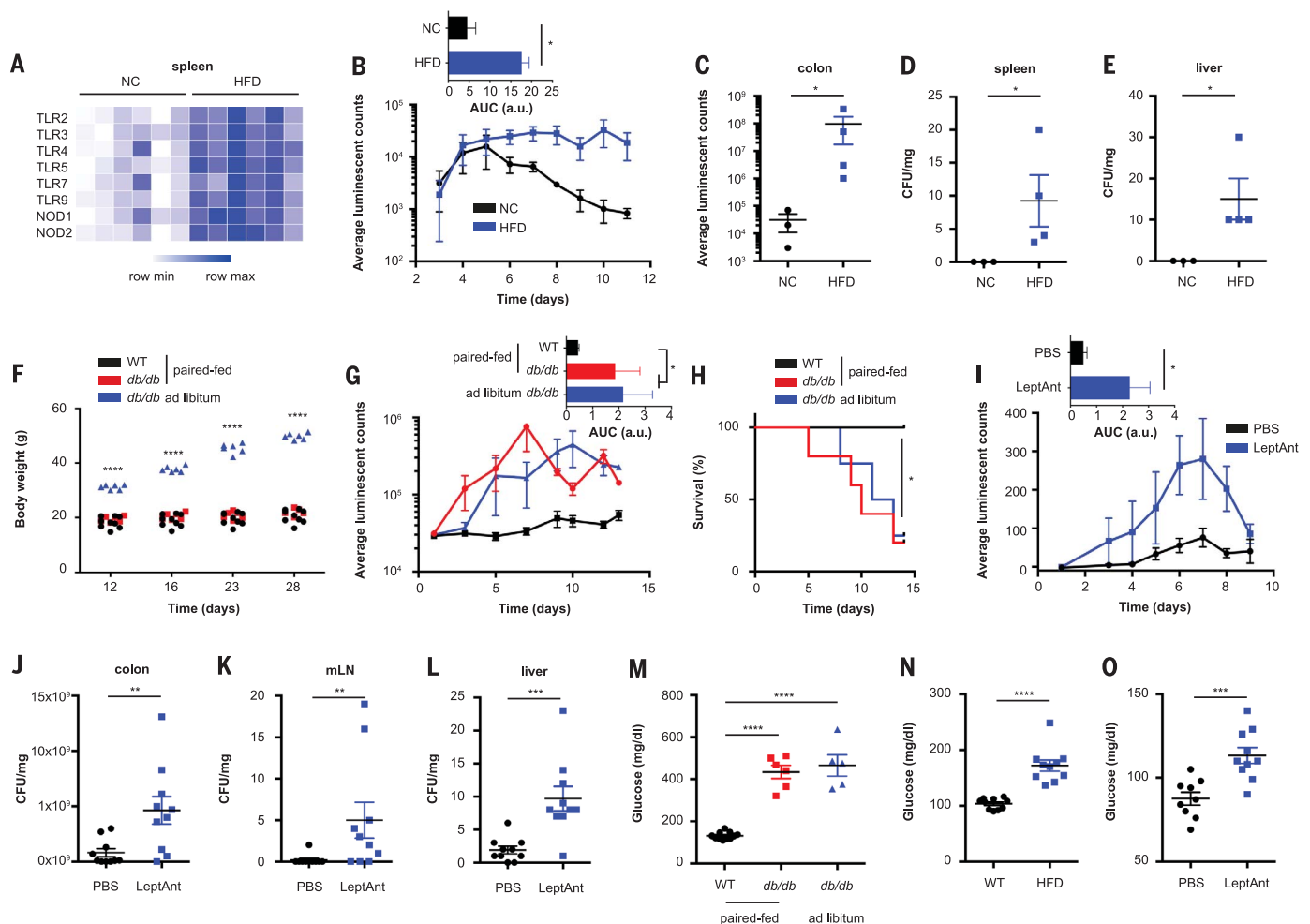


**Fig. 2. Obesity does not suffice to explain susceptibility to enteric infection.** (A) PRR stimulation by splenic extracts from mice fed a high-fat diet (HFD). (B to E) Abdominal luminescence (B) and CFUs recovered from colonic tissue (C), spleens (D), and livers (E) of HFD-fed mice infected with luminescent *C. rodentium*. (F to H) Body weight (F), *C. rodentium* luminescence (G), and *C. rodentium*-induced mortality (H) in paired-fed *db/db* mice and controls. (I to L) Total abdominal luminescence signals (I)

and live CFUs recovered from colonic tissue (J), mesenteric lymph nodes (K) and livers (L) from leptin antagonist (LeptAnt)-treated mice infected with bioluminescent *C. rodentium*. (M to O) Blood glucose concentrations in paired-fed *db/db* mice (M), HFD-fed mice (N), and LeptAnt-treated mice (O). All data represent at least two independent experiments. Means  $\pm$  SEM are plotted. \* $P < 0.05$ , \*\* $P < 0.01$ , \*\*\* $P < 0.001$ , \*\*\*\* $P < 0.0001$  by ANOVA (F and M) or Mann-Whitney *U* test (all other panels).

donors and controls to normoglycemic germ-free mice neither induced dissemination of bacterial products to systemic sites (fig. S6E) nor increased susceptibility to *C. rodentium* infection (fig. S6, F to J). These data indicate that although the commensal microbiota serves as the reservoir of microbial molecules that translocate to the systemic circulation upon disruption of the intestinal barrier, compositional microbiota alterations arising under hyperglycemic conditions do not directly affect barrier integrity.

To corroborate the specificity of hyperglycemia as a driver of susceptibility to intestinal infection, we used hyperglycemic *Akita* mice (fig. S7A), an STZ-independent model of type I diabetes mellitus that harbors a spontaneous mutation in the gene encoding insulin 2 (20). As in STZ-treated mice, we observed in this model elevated *C. rodentium* growth and pathogenic translocation to systemic tissues (Fig. 3, M and N, and fig. S7, B and C). To further validate the specific impact of hyperglycemia as a driver of the barrier dysfunction phenotype, we administered 0.25 U per day of insulin to STZ-

treated mice via hyperosmotic pumps for 4 weeks, which restored normoglycemic levels (fig. S7D). Treatment with insulin also prevented the loss of adherence junction integrity (Fig. 4A and fig. S7E), systemic dissemination of microbial products (Fig. 4B), and enhanced *C. rodentium* growth and pathogenic translocation (Fig. 4, C and D). Together, these experiments establish hyperglycemia as a direct and specific cause for intestinal barrier dysfunction and susceptibility to enteric infection.

### Hyperglycemia reprograms intestinal epithelial cells

To determine whether glucose acted directly on intestinal epithelial cells to affect barrier function, we used an *in vitro* system of cultured intestinal epithelial (Caco-2) cells exposed to different concentrations of glucose in the culture medium. We assessed tight junction integrity through automated high-throughput analysis of ZO-1 staining patterns. Indeed, glucose induced barrier alterations in a dose- and time-dependent manner, manifesting visually as increased tortuosity and

altered appearance of cell-cell junctions (Fig. 4, E to H). To investigate the mechanisms by which elevated blood glucose concentrations compromise intestinal epithelial cell function *in vivo*, we performed RNA sequencing of purified intestinal epithelial cells from STZ-treated mice and controls. Global reprogramming of the epithelial transcriptome was detected in hyperglycemic mice (Fig. 4I), in which more than 1000 genes were differentially expressed compared to vehicle-treated controls (Fig. 4J). These genes were predominantly involved in metabolic pathways, and specifically in N-glycan biosynthesis and pentose-glucuronate interconversion (Fig. 4K), two intracellular functions critically involved in the maintenance of epithelial barrier function (21–29). For example, hyperglycemia affected the entire pathway of protein N-glycosylation by provoking marked downregulation of central genes (Fig. 4L and fig. S8). In contrast, epithelial proliferation or cell death were not affected by STZ treatment (fig. S9, A to D).

In addition to the above epithelial changes, hyperglycemia modestly affected the intestinal

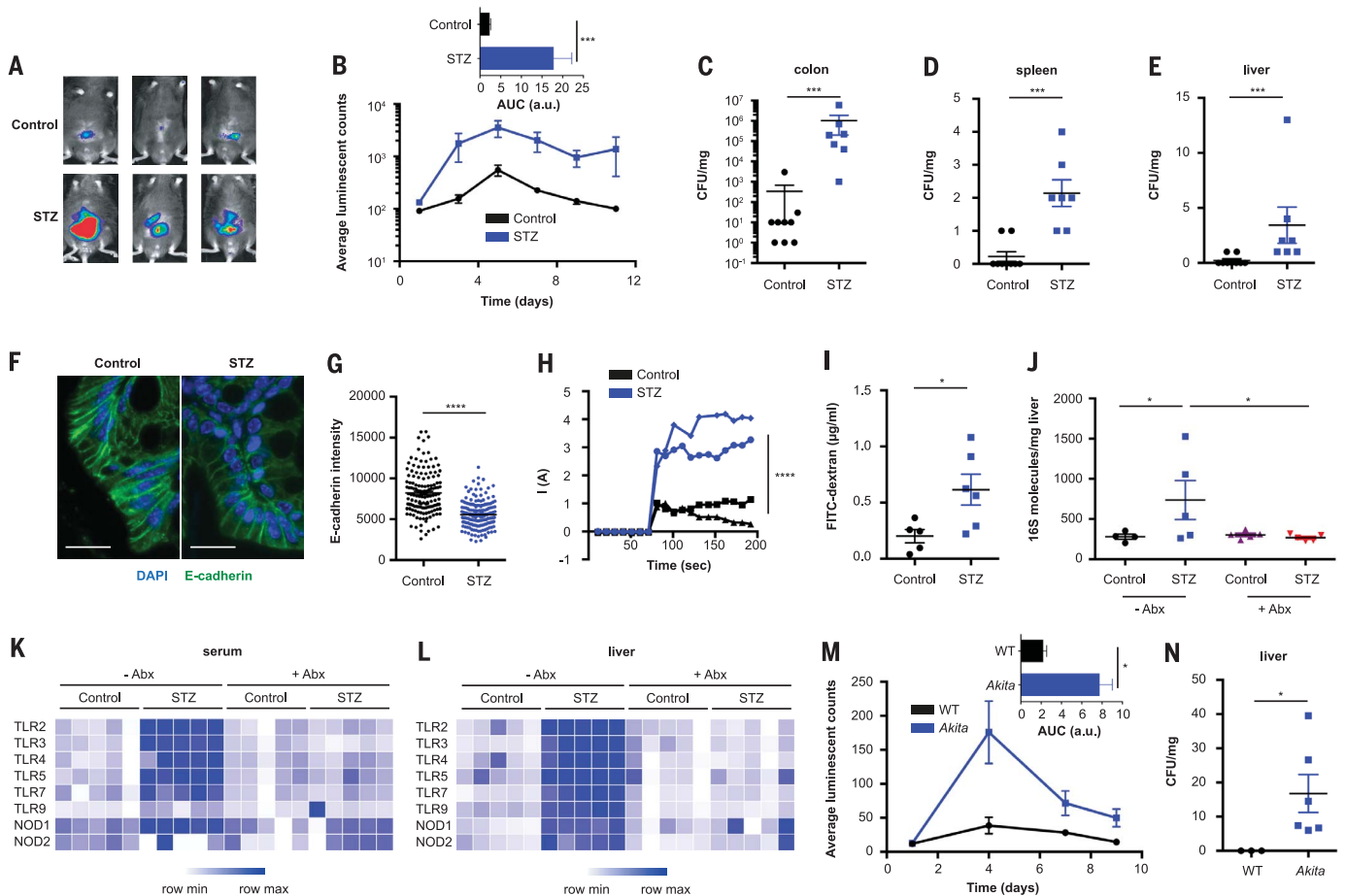


### Fig. 3. Hyperglycemia causes susceptibility to enteric infection.

(A to E) Abdominal luminescence (A and B) and CFUs recovered from colonic tissue (C), spleens (D), and livers (E) from STZ-treated mice infected with bioluminescent *C. rodentium*. (F and G) E-cadherin staining (F) and quantification (G) of colons from STZ-treated mice and controls. Scale bars, 25 µm. (H) Ussing chamber recordings from colons of STZ-treated mice and controls. (I) FITC-dextran recovered from the serum of STZ-treated mice

after oral gavage. (J) Detection of 16S rDNA in livers of STZ- and Abx-treated mice. (K and L) PRR stimulation by sera (K) and hepatic extracts (L) from STZ-treated mice and controls, with or without antibiotic (Abx) treatment. (M and N) Abdominal luminescence (M) and hepatic CFUs (N) from *C. rodentium*-infected *Akita* mice. All data represent at least two independent experiments. Means ± SEM are plotted. \* $P < 0.05$ , \*\*\* $P < 0.001$ , \*\*\*\* $P < 0.0001$  by ANOVA (J) or Mann-Whitney *U* test (all other panels).

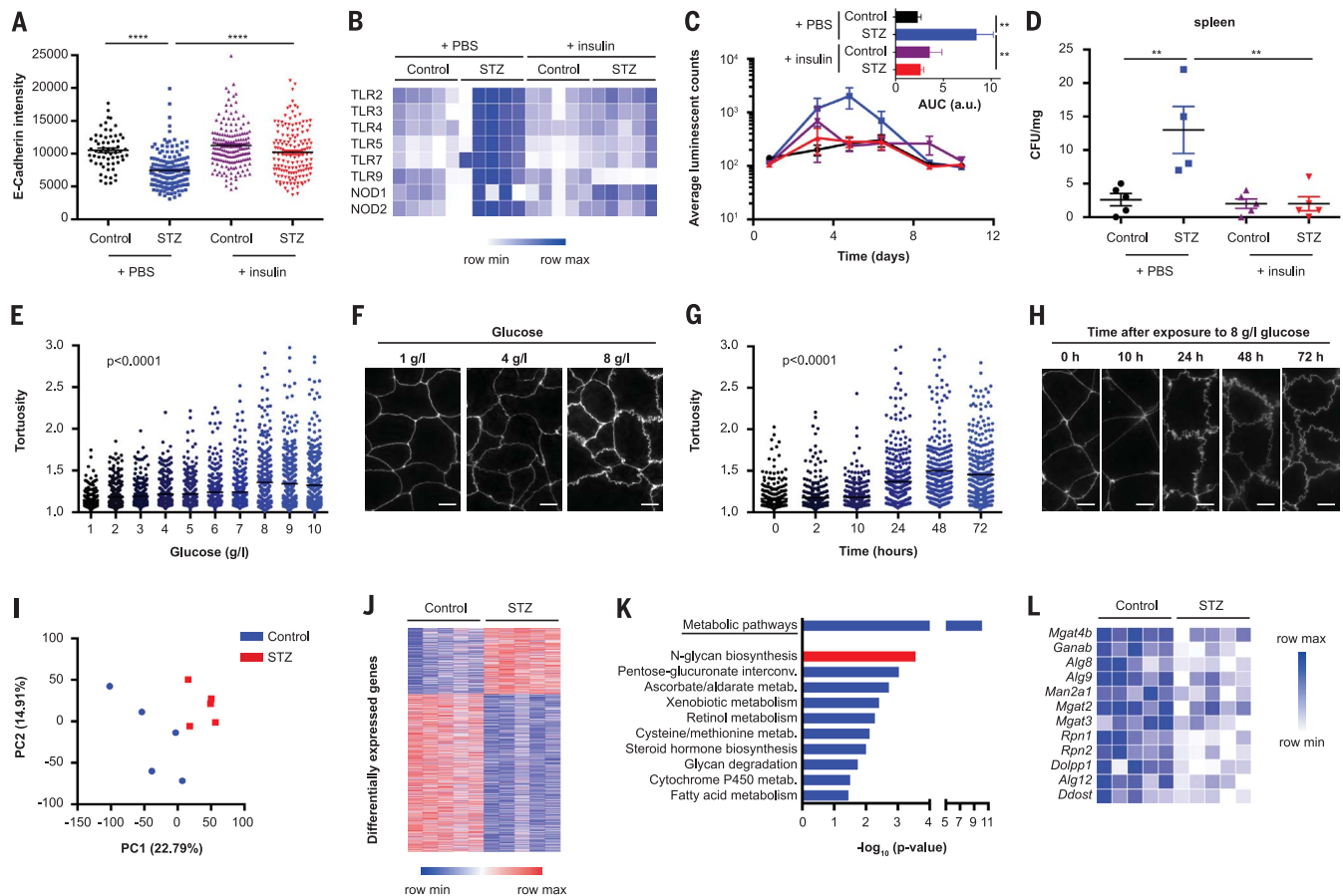


**Fig. 4. Hyperglycemia alters intestinal epithelial cell function.**

(A and B) Colonic E-cadherin intensity (A) and PRR ligand stimulation by sera (B) from STZ-treated mice and controls, with or without insulin administration. (C and D) Abdominal luminescence (C) and CFUs recovered from the spleen (D) of STZ- and insulin-treated mice after *C. rodentium* infection. (E to H) Quantification of barrier tortuosity (E and G) and representative ZO-1 staining (F and H) of Caco-2 cells

and splenic immune system, specifically by causing an increased representation of myeloid cells (fig. S10, A to J), in line with previous reports (30). However, STZ treatment did not provoke an overt inflammatory state in the intestine (fig. S11, A to E). In particular, cytokines involved in interleukin-22 (IL-22)-mediated barrier function and host defense, which has been implicated in the susceptibility of obese mice to infection (12), were unaltered, as was the epithelial transcriptional response to IL-22 (fig. S11F). Indeed, hyperglycemia and IL-22 appeared to have additive effects in mediating host defense against *C. rodentium*, because STZ-treated IL-22-deficient mice featured accelerated bacterial growth and mortality when compared to IL-22-deficient controls (fig. S11, G and H). We further compared the involvement of epithelial and immune cells in host defense against another gastrointestinal pathogen, *Salmonella* Typhimurium. STZ-treated mice orally infected with *Salmonella* showed enhanced systemic colonization, whereas intestinal luminal growth was comparable to that of vehicle-

treated controls (fig. S12, A to E). In contrast to this marked susceptibility of STZ-treated mice to oral *Salmonella* Typhimurium infection, susceptibility of these mice to systemic infection was only apparent in the liver (fig. S12, F to H). Notably, systemic infection with *Salmonella* caused enhanced intestinal colonization in STZ-treated mice, potentially indicative of retrograde spread of bacteria across a compromised barrier (fig. S12, I and J).

#### Epithelial reprogramming by hyperglycemia involves glucose metabolism and GLUT2

We next assessed whether epithelial glucose metabolism was involved in the transcriptional reprogramming of STZ-treated mice. Isolated intestinal epithelial cells from hyperglycemic mice featured elevated amounts of metabolites along the glycolytic cascade (fig. S13A). Inhibition of glucose metabolism via 2-deoxyglucose (2-DG) rescued glucose-induced barrier aberrations in vitro in a dose-dependent manner (Fig. 5, A to

C). In addition, 2-DG administration blocked transcriptional reprogramming in STZ-treated mice (Fig. 5D and fig. S13B), including the N-glycan pathway (fig. S13C); prevented the systemic dissemination of microbial products (Fig. 5, E and F); and restored host defense against *C. rodentium* (Fig. 5G and fig. S13, D to F). Bacterial growth in the intestinal lumen was unaffected by 2-DG treatment (fig. S13G). To test whether 2-DG could be used to counteract hyperglycemia-mediated loss of barrier integrity beyond the STZ model, we administered 2-DG to *C. rodentium*-infected *db/db* mice and assessed its impact on systemic dissemination of the pathogen. Notably, the detectable pathogen load in the mesenteric lymph nodes, spleens, and livers of 2-DG-treated *db/db* mice was strongly reduced under 2-DG treatment (Fig. 5H and fig. S13, H and I). Together, these data suggest that glucose-mediated reprogramming of epithelial cell metabolic function leads to transcriptional alterations, abrogation of the intestinal barrier, and impaired host defense against enteric infection.

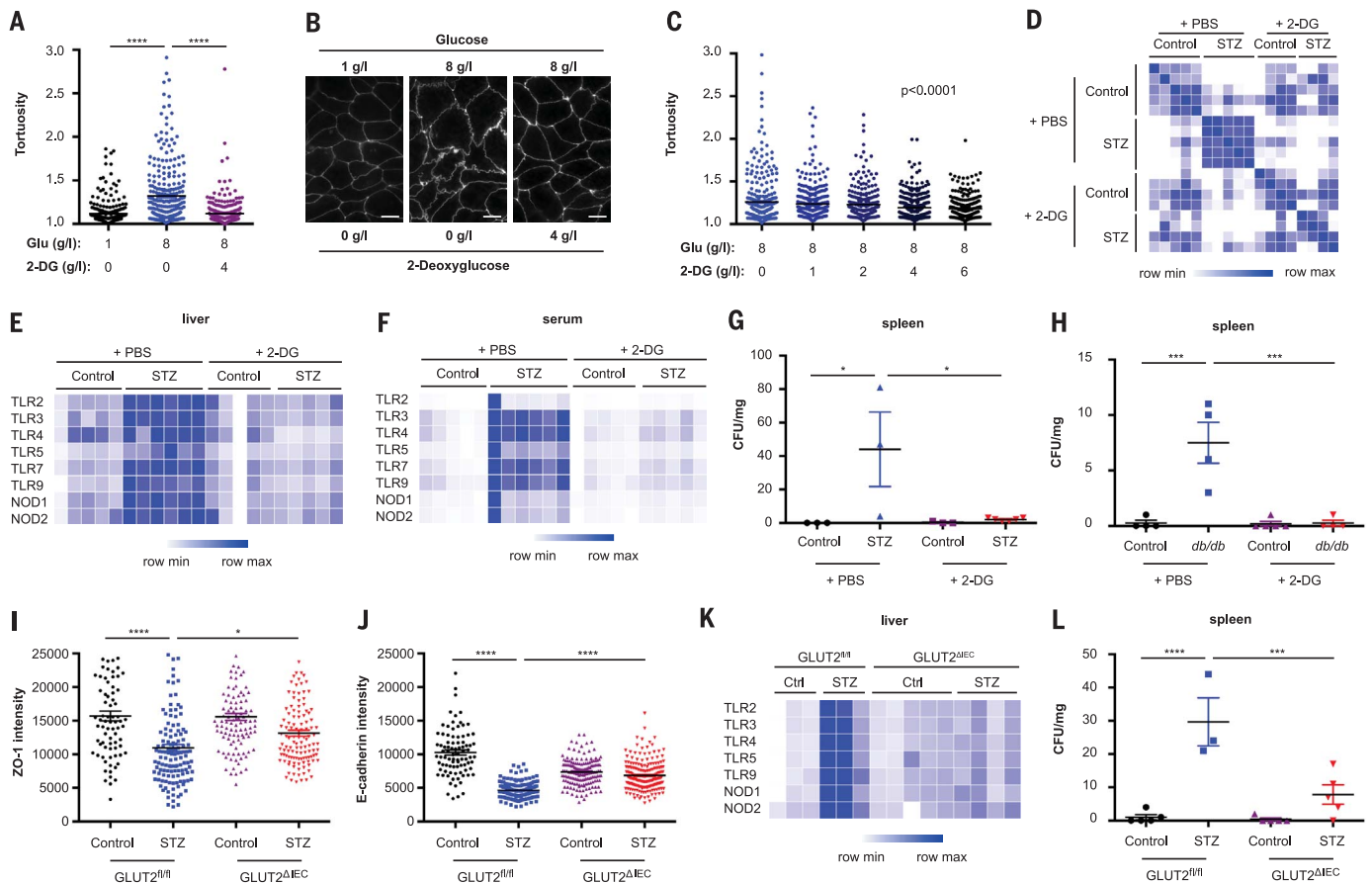


**Fig. 5. Epithelial reprogramming by hyperglycemia involves glucose metabolism and GLUT2.** (A to C) Quantification of barrier tortuosity (A and C) and representative ZO-1 staining (B) of Caco-2 cells treated with the indicated concentrations of glucose and 2-deoxyglucose (2-DG). Scale bars, 10  $\mu$ m. (D) Similarity matrix of the epithelial transcriptomes of STZ-treated mice, with or without 2-DG administration. (E and F) PRR stimulation by hepatic extracts (E) and sera (F) from STZ-treated mice, with or without 2-DG

administration. (G and H) Splenic CFUs from *C. rodentium*-infected and 2-DG-treated STZ (G) and *db/db* mice (H). (I to K) Colonic ZO-1 (I) and E-cadherin intensity (J) and PRR stimulation by hepatic extracts (K) from STZ-treated GLUT2 $\Delta$ IEC mice and controls. (L) CFUs recovered from spleens of STZ-treated GLUT2 $\Delta$ IEC mice and controls infected with *C. rodentium*. All data represent at least two independent experiments. Means  $\pm$  SEM are plotted. \* $P < 0.05$ , \*\* $P < 0.01$ , \*\*\* $P < 0.001$ , \*\*\*\* $P < 0.0001$  by ANOVA.

Glucose transport between the intestinal epithelium and circulation is mediated by the bidirectional glucose transporter GLUT2 (31). To determine the role of this transporter in hyperglycemia-mediated epithelial reprogramming, we next used mice selectively lacking GLUT2 in intestinal epithelial cells (GLUT2 $\Delta$ IEC) (32) and induced hyperglycemia in these mice by STZ administration. Indeed, GLUT2 $\Delta$ IEC mice were resistant to STZ-induced transcriptional reprogramming and retained epithelial transcriptomes similar to those of controls (fig. S14, A and B). GLUT2 $\Delta$ IEC mice also retained intact tight and adherence junction complexes (Fig. 5, I and J, and fig. S14, C and D), reduced transepithelial flux (fig. S14E), and intestinal containment of microbial PRR ligands (Fig. 5K), despite sustained STZ-induced hyperglycemia (fig. S14F). Ablation of GLUT2 also ameliorated the STZ-induced susceptibility to *C. rodentium* growth and systemic dissemination (Fig. 5 L, and fig. S14, G to I). Collectively, these results indicate that GLUT2 is involved in the hyperglycemia-induced metabolic and transcriptional alterations in intestinal epi-

thelial cells, resulting in barrier dysfunction and microbial translocation to the systemic circulation.

### Blood glucose concentrations are associated with microbial product influx in humans

Finally, we sought to determine whether glycaemic levels similarly correlate with intestinal barrier function in humans. To this end, we recruited 27 healthy individuals (fig. S15, A and B) and performed measurements of multiple serum parameters and microbial products in the circulation. Of all variables measured, hemoglobin A1c (HbA1c), indicative of an individual's 3-month average plasma glucose concentration, showed the strongest correlation with serum levels of PRR ligands (Fig. 6, A to C, and fig. S15, C to E). In contrast, high body mass index and other hallmarks of metabolic disease did not significantly associate with the influx of microbial products (Fig. 6, A and B, and fig. S15F). Total stool bacterial content did not correlate with HbA1c levels (fig. S15G). Together, these data suggest that similar to their effects in mice, serum glucose

concentrations, rather than obesity, may associate with or potentially even drive intestinal barrier dysfunction in humans.

### Discussion

Serum glucose is among the most strictly controlled physiological variables of organismal homeostasis. Chronically elevated glucose concentrations, as observed in diabetes mellitus, obesity, and associated metabolic disorders, such as non-alcoholic fatty liver disease, result from altered homeostatic set points of the tightly regulated normoglycemic levels (33). Long-standing hyperglycemia, in turn, leads to a myriad of potentially devastating biochemical and physiological consequences, such as the generation of advanced glycation end products, pancreatic glucose toxicity (34, 35), macrovascular and microvascular complications affecting virtually every organ (36), risk of infection (37), and enhanced mortality (38).

In this study, we have identified glucose as an orchestrator of intestinal barrier function. Hyperglycemia markedly interfered with homeostatic epithelial integrity, leading to abnormal influx of

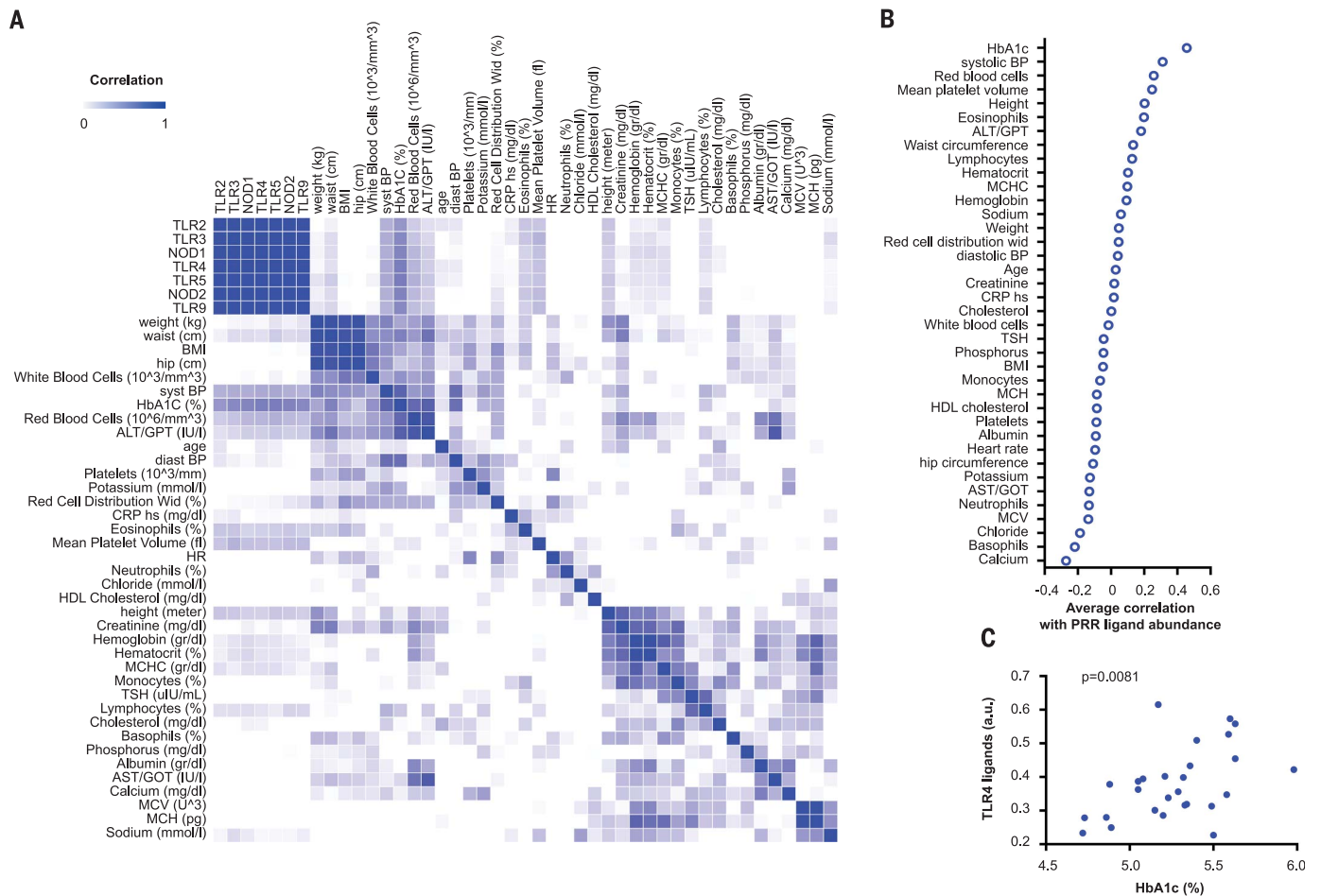


**Fig. 6. Hyperglycemia is associated with influx of microbial products in humans.** (A and B) Correlation matrix (A) and average correlations with systemic PRR ligands (B) of the indicated parameters in the serum of 27 healthy volunteers. (C) Correlation of HbA1c with serum levels of TLR4 ligands.

immune-stimulatory microbial products and a propensity for systemic spread of enteric pathogens. Our results indicate that hyperglycemia causes retrograde transport of glucose into intestinal epithelial cells via GLUT2, followed by alterations in intracellular glucose metabolism and transcriptional reprogramming (fig. S16). One of the most strongly affected pathways by hyperglycemia in our study involves the N-glycosylation of proteins in the endoplasmic reticulum and Golgi apparatus, which has been implicated as a key regulator of a multitude of epithelial functions (25). Although our study focused on the impact of systemic glucose concentrations on the intestinal barrier, similar effects might be caused by a high-glucose diet, which may affect intestinal epithelial cells in a similar manner, potentially resulting in diet-induced alterations of barrier function. Such potential physiologically important dietary effects on barrier function merit further studies. Furthermore, the impact of hyperglycemia on epithelial barrier function might be relevant beyond the gastrointestinal tract and affect other mucosal surfaces, such as the respiratory tract, as was indicated by a recent study of close to 70,000 diabetes patients highlighting a positive corre-

lation between HbA1c values and a variety of mucosal community- and hospital-acquired infections (39).

Collectively, our findings provide a potential molecular explanation for altered barrier function in the context of the metabolic syndrome and the resultant enhanced mucosal infection noted in patients suffering from obesity (5) and diabetes mellitus (40). Furthermore, the link that we highlight between hyperglycemia and gut barrier alterations may provide a mechanistic basis for a variety of seemingly unrelated inflammatory manifestations, complications, and associations of the metabolic syndrome—collectively termed “metaflammation” or “para-inflammation” (41, 42). Examples of these include adipose tissue inflammation driving exacerbated obesity and glucose intolerance (43), nonalcoholic fatty liver disease progressing to detrimental nonalcoholic steatohepatitis (44), inflammation contributing to atherosclerosis and associated cardiovascular disease (45), and even recently suggested associations between the metabolic syndrome and neurodegeneration (46). Ultimately, our results may present the starting point for harnessing glucose metabolism or other regulators of intestinal barrier integrity as potential therapeutic targets in

the prevention and amelioration of enteric infection and gut-related systemic inflammation.

**REFERENCES AND NOTES**

1. N. Stefan, F. Schick, H. U. Häring, *Cell Metab.* **26**, 292–300 (2017).
2. D. A. Winer, H. Luck, S. Tsai, S. Winer, *Cell Metab.* **23**, 413–426 (2016).
3. P. D. Cani *et al.*, *Diabetes* **57**, 1470–1481 (2008).
4. M. E. Falagas, M. Kompoti, *Lancet Infect. Dis.* **6**, 438–446 (2006).
5. K. A. Kaspersen *et al.*, *Epidemiology* **26**, 580–589 (2015).
6. J. Casqueiro, J. Casqueiro, C. Alves, *Indian J. Endocrinol. Metab.* **16** (suppl. S1), 27–36 (2012).
7. S. I. Grivennikov *et al.*, *Nature* **491**, 254–258 (2012).
8. T. R. Sampson *et al.*, *Cell* **167**, 1469–1480.e12 (2016).
9. N. Thevaranjan *et al.*, *Cell Host Microbe* **21**, 455–466.e4 (2017).
10. R. Ahmad, B. Rah, D. Bastola, P. Dhawan, A. B. Singh, *Sci. Rep.* **7**, 5125 (2017).
11. N. M. Mackey-Lawrence, W. A. Petri Jr., *Mucosal Immunol.* **5**, 472–479 (2012).
12. X. Wang *et al.*, *Nature* **514**, 237–241 (2014).
13. R. Madan *et al.*, *Infect. Immun.* **82**, 341–349 (2014).
14. C. Guillot, T. Lecuit, *Science* **340**, 1185–1189 (2013).
15. J. W. Collins *et al.*, *Nat. Rev. Microbiol.* **12**, 612–623 (2014).
16. M. Wlodarska *et al.*, *Cell* **156**, 1045–1059 (2014).
17. M. G. Myers Jr., H. Münzberg, G. M. Leininger, R. L. Leshan, *Cell Metab.* **9**, 117–123 (2009).
18. E. Elinav *et al.*, *Endocrinology* **150**, 3083–3091 (2009).
19. M. S. Islam, D. T. Loots, *Methods Find. Exp. Clin. Pharmacol.* **31**, 249–261 (2009).
20. J. Wang *et al.*, *J. Clin. Invest.* **103**, 27–37 (1999).
21. D. W. Scott *et al.*, *Mol. Biol. Cell* **26**, 3205–3214 (2015).
22. M. Nita-Lazar, I. Rebutini, J. Walker, M. A. Kukuruzinska, *Exp. Cell Res.* **316**, 1871–1884 (2010).

23. B. T. Jamal *et al.*, *Cell Health Cytoskelet.* **2009**, 67–80 (2009).
24. Y. Goto *et al.*, *Science* **345**, 1254009 (2014).
25. Y. Goto, S. Uematsu, H. Kiyono, *Nat. Immunol.* **17**, 1244–1251 (2016).
26. T. A. Pham *et al.*, *Cell Host Microbe* **16**, 504–516 (2014).
27. J. M. Pickard *et al.*, *Nature* **514**, 638–641 (2014).
28. K. S. Bergstrom *et al.*, *PLoS Pathog.* **6**, e1000902 (2010).
29. M. Van der Sluis *et al.*, *Gastroenterology* **131**, 117–129 (2006).
30. S. Niu *et al.*, *J. Immunol.* **197**, 3293–3301 (2016).
31. B. Thorens, *Diabetologia* **58**, 221–232 (2015).
32. C. C. Schmitt *et al.*, *Mol. Metab.* **6**, 61–72 (2016).
33. M. E. Kotas, R. Medzhitov, *Cell* **160**, 816–827 (2015).
34. A. Bangert *et al.*, *Proc. Natl. Acad. Sci. U.S.A.* **113**, E155–E164 (2016).
35. Y. Tanaka, P. O. Tran, J. Harmon, R. P. Robertson, *Proc. Natl. Acad. Sci. U.S.A.* **99**, 12363–12368 (2002).
36. R. Madonna, R. De Caterina, *Vascul. Pharmacol.* **54**, 68–74 (2011).
37. S. O. Butler, I. F. Btaiche, C. Alaniz, *Pharmacotherapy* **25**, 963–976 (2005).
38. S. A. Leite *et al.*, *Diabetol. Metab. Syndr.* **2**, 49 (2010).
39. A. Mor *et al.*, *Am. J. Epidemiol.* **186**, 227–236 (2017).
40. L. M. Muller *et al.*, *Clin. Infect Dis.* **41**, 281–288 (2005).
41. R. Medzhitov, *Nature* **454**, 428–435 (2008).
42. G. S. Hotamisligil, *Nature* **542**, 177–185 (2017).
43. D. Okin, R. Medzhitov, *Cell* **165**, 343–356 (2016).
44. A. Nakamura *et al.*, *J. Diabetes Investig.* **2**, 483–489 (2011).
45. F. Pistrosch, A. Natali, M. Hanefeld, *Diabetes Care* **34** (suppl. 2), S128–S131 (2011).
46. M. Barbagallo, L. J. Dominguez, *World J. Diabetes* **5**, 889–893 (2014).

#### ACKNOWLEDGMENTS

We thank the members of the Elinav lab for discussions, J. Friedman for providing mice, and A. Erez and S. Limanovich for helpful advice.

**Funding:** C.A.T. received a Boehringer Ingelheim Fonds PhD Fellowship. B.G. holds the Erwin Neter professorial Chair in cell and tumor biology. B.G. and E.E. are supported by the Leona M. and Harry B. Helmsley Charitable Trust; E.E. is supported by Y. and R. Ungar; the Adelis Foundation; the Gurwin Family Fund for Scientific Research; the Crown Endowment Fund for Immunological Research; the estate of J. Gitlitz; the estate of L. Hershkovich; the Benozio Endowment Fund for the Advancement of Science; J. L. and V. Schwartz; A. and G. Markovitz; A. and C. Adelson; the French National Center for Scientific Research (CNRS); D. L. Schwarz; the V. R. Schwartz Research Fellow Chair; L. Steinberg; J. N. Halpern; A. Edelheit; and by grants funded by the European Research Council; a Marie Curie Integration grant; the German-Israeli Foundation for Scientific Research and Development; the Israel Science Foundation; the Helmholtz Foundation; and the European Foundation for the Study of Diabetes. P.S. and A.G. acknowledge ANR-ALIA 007-01 Nutra2-sense for the generation of the intestinal epithelial-specific GLUT2 knockout mice. E.E. holds the Sir Marc & Lady Tania Feldmann professorial Chair in immunology, is a senior fellow of the Canadian Institute for Advanced Research (CIFAR), and an international researcher of the Bill & Melinda Gates Foundation and Howard Hughes Medical Institute (HHMI). **Author contributions:** C.A.T. conceived the study; designed, performed, analyzed, and interpreted experiments; and wrote the manuscript. M.L., I.G., D.Z., E.S., E.B., S.B., A.C.T., M.N.K. and M.P.-F. performed and analyzed

experiments. O.B., M.E., R.B.-Z., D.L.-R., Z.H., and S.A. carried out the human study. A.G., A.H., P.S., A.G., H.G., and B.G. provided critical tools, insights, and advice. E.E. conceived the study, supervised and mentored its participants, interpreted results, and wrote the manuscript. **Competing interests:** The authors declare that they have no competing interests. **Data and materials availability:** All data and code to understand and assess the conclusions of this research are available in the main text, supplementary materials, and via the following repositories: European Nucleotide Archive (ENA) accession no. PRJEB24760. This work is licensed under a Creative Commons Attribution 4.0 International (CC BY 4.0) license, which permits unrestricted use, distribution, and reproduction in any medium, provided the original work is properly cited. To view a copy of this license, visit <http://creativecommons.org/licenses/by/4.0/>. This license does not apply to figures/photos/artwork or other content included in the article that is credited to a third party; obtain authorization from the rights holder before using such material.

#### SUPPLEMENTARY MATERIALS

[www.sciencemag.org/content/359/6382/1376/suppl/DC1](http://www.sciencemag.org/content/359/6382/1376/suppl/DC1)  
Materials and Methods  
Figs. S1 to S16  
References (47–56)

26 October 2017; accepted 6 February 2018  
Published online 8 March 2018  
10.1126/science.aar3318

## Hyperglycemia drives intestinal barrier dysfunction and risk for enteric infection

Christoph A. Thaiss, Maayan Levy, Inna Grosheva, Danping Zheng, Eliran Soffer, Eran Blacher, Sofia Braverman, Anouk C. Tengeler, Oren Barak, Maya Elazar, Rotem Ben-Zeev, Dana Lehavi-Regev, Meirav N. Katz, Meirav Pevsner-Fischer, Arieh Gertler, Zamir Halpern, Alon Harmelin, Suhail Amar, Patricia Serradas, Alexandra Grosfeld, Hagit Shapiro, Benjamin Geiger and Eran Elinav

*Science* **359** (6382), 1376-1383.

DOI: 10.1126/science.aar3318 originally published online March 8, 2018

### Metabolic syndrome, leaky guts, and infection

Metabolic syndrome often accompanies obesity and hyperglycemia and is associated with a breakdown in the integrity of the intestinal barrier and increased risk of systemic infection. Thaiss *et al.* found that mice with systemic infection of a *Salmonella* analog, *Citrobacter rodentium*, also exhibited hyperglycemia. Deletion of the glucose transporter GLUT2 altered sensitivity to chemically induced epithelial permeability and protected mice from pathogen invasion. The authors also found a correlation in humans between glycated hemoglobin (an indicator of hyperglycemia) and serum levels of pathogen recognition receptor ligands.

*Science*, this issue p. 1376

#### ARTICLE TOOLS

<http://science.sciencemag.org/content/359/6382/1376>

#### SUPPLEMENTARY MATERIALS

<http://science.sciencemag.org/content/suppl/2018/03/07/science.aar3318.DC1>

#### RELATED CONTENT

<http://science.sciencemag.org/content/sci/359/6380/1156.full>  
<http://science.sciencemag.org/content/sci/359/6380/1161.full>  
<http://science.sciencemag.org/content/sci/359/6380/1097.full>  
<http://stm.sciencemag.org/content/scitransmed/6/237/237fs22.full>  
<http://stm.sciencemag.org/content/scitransmed/6/237/237ra66.full>  
<http://stm.sciencemag.org/content/scitransmed/9/386/eaag2513.full>  
<http://stm.sciencemag.org/content/scitransmed/9/379/eaaf6397.full>

#### REFERENCES

This article cites 56 articles, 11 of which you can access for free  
<http://science.sciencemag.org/content/359/6382/1376#BIBL>

#### PERMISSIONS

<http://www.sciencemag.org/help/reprints-and-permissions>

Use of this article is subject to the [Terms of Service](#)



## Supplementary Materials for

### **Hyperglycemia drives intestinal barrier dysfunction and risk for enteric infection**

Christoph A. Thaiss, Maayan Levy, Inna Grosheva, Danping Zheng, Eliran Soffer, Eran Blacher, Sofia Braverman, Anouk C. Tengeler, Oren Barak, Maya Elazar, Rotem Ben-Zeev, Dana Lehavi-Regev, Meirav N. Katz, Meirav Pevsner-Fischer, Arie Gertler, Zamir Halpern, Alon Harmelin, Suhail Amar, Patricia Serradas, Alexandra Grosfeld, Hagit Shapiro, Benjamin Geiger, Eran Elinav\*

\*Corresponding author. E-mail: [eran.elinav@weizmann.ac.il](mailto:eran.elinav@weizmann.ac.il)

Published 8 March 2018 on *Science* First Release  
DOI: 10.1126/science.aar3318

#### **This PDF file includes:**

Materials and Methods  
Figs. S1 to S16  
References

## Supporting Online Material

### Materials and methods

#### Mice

Wild-type C57Bl/6 mice were purchased from Harlan and allowed to acclimatize to the animal facility environment for 2 weeks before used for experimentation. Germ-free C57Bl/6 mice were born in the Weizmann Institute germ-free facility and routinely monitored for sterility. The following genetically modified mice were obtained from the Jackson Laboratory: B6.BKS(D)-Lepr<sup>db</sup>/J, B6.Cg-Lep<sup>ob</sup>/J, B6.Cg-Tg(Vil1-cre)1000Gum/J, B6.Cg-Tg(Alb-cre)21Mgn/J, B6.Cg-Tg(Nes-cre)1Kln/J, C57BL/6-Ins2<sup>Akita</sup>/J. Sim1-Cre, SF1-Cre, ChAT-Cre, POMC-Cre, and AgRP-Cre mice were kindly provided by Yael Kuperman (Weizmann Institute). LepR-flox mice were generously provided by Jeffrey Friedman (Rockefeller University). Villin-Cre:GLUT2<sup>fl/fl</sup> mice on a C57BL/6 background were kindly provided by Patricia Serradas and Alexandra Grosfeld (Université Pierre et Marie Curie) and maintained as previously reported (32).

In each experiment, all mice were littermates born and raised in the same vivarium. In all experiments, age- and gender-matched mice were used. All mice were maintained on a strict 12-h light-dark cycle (lights turned on at 6 am and turned off at 6 pm) and were housed in cages containing a maximum of five animals.

Before dietary interventions, mice were randomized to ensure that no incidental pre-diet differences in body weight existed between the different groups. Mice were exposed to high-fat diet for 12 weeks (Open Source Diets D12492) or normal chow diet (Teklad 2018) as indicated. In paired-feeding experiments, the food consumed by the wild-type group was weighted daily, and the same amount of food was made available to the *db/db* group for the subsequent day.

To induce hyperglycemia, streptozotocin (STZ, Sigma-Aldrich) was diluted freshly in PBS and injected i.p. at 100 mg/kg at two consecutive days. Control mice were injected with PBS. Serum glucose measurements were performed using glucose strips (Perrigo). Hyperglycemic mice were used for further experimentation 2-3 weeks after STZ injection). For continuous insulin administration, ALZET osmotic pumps were used. Pumps were implanted subcutaneously in the back of the mice for 4 weeks. Insulin was delivered at 0.25 U/day. 2-deoxyglucose (2-DG) was injected i.p. twice daily at 5 mg per injection as previously described (47). Injections were performed for 10 consecutive days. Leptin antagonist was administered daily by intraperitoneal injection of 25 mg/kg as previously described (18).

Fresh stool samples from mice were collected in tubes, immediately frozen in liquid nitrogen upon collection, and stored at -80°C until DNA isolation. For antibiotic treatment, mice were given a combination of vancomycin (1 g/l), ampicillin (1 g/l), kanamycin (1 g/l), and metronidazole (1 g/l) in their drinking water (48). All antibiotics were obtained from Sigma Aldrich. For fecal transplantation experiments, microbiota samples were collected and homogenized under anaerobic conditions. Homogenized samples were filtered through a 70 µm mesh and administered to germ-free recipients by oral gavage of 200 µl.

All experiments were approved by the local IACUC.

### ***Citrobacter rodentium* infection**

Mice were infected by oral gavage with 200 µl of an overnight culture of LB containing approximately  $1 \times 10^9$  colony-forming units (CFU) of a kanamycin-resistant, luciferase-expressing derivative of *C. rodentium* DBS100 (ICC180) as previously described (16). For *in vivo* bioluminescent imaging, mice were anesthetized with Ketamine/Xylazine. Bioluminescence was quantified using an IVIS2000 instrument and Living Image software (Perkin Elmer). For *ex vivo* luminescence analysis, colons were resected, extensively washed from all fecal matter and immediately imaged. For CFU counts, tissues were collected, weighed and homogenized in 1 ml of sterile PBS. Tissue homogenates were serially diluted in PBS and plated on to LB kanamycin plates, incubated overnight at 37°C, and bacterial colonies were enumerated the following day, normalizing them to the tissue weight.

### ***Salmonella* Typhimurium infection**

For oral infections, mice were pretreated with 50 mg/ml streptomycin one day prior to oral gavage of  $10^8$  CFU of SPI-II-deficient *Salmonella* Typhimurium (49). For systemic infections, mice were injected  $10^4$  CFU of *Salmonella* Typhimurium by intraperitoneal injection as previously described (50). One week after infection, colonization was assessed by bacterial plating on LB streptomycin plates, incubated overnight at 37°C, and bacterial colonies were enumerated the following day, normalizing them to the tissue weight.

### **Quantification of microbial products at systemic sites**

The following PRR reporter cell lines were obtained from Invivogen (HEK-Blue TLR and NLR reporter cell lines): TLR2, TLR3, TLR4, TLR5, TLR7, TLR9, NOD1, NOD2. Extracts from spleen, liver, and serum were homogenized and added to reporter cell lines incubated with HEK-Blue detection medium (Invivogen) according to the manufacturer's instructions.

### **16S qPCR for quantification of bacterial DNA**

DNA was extracted from samples using MoBio PowerSoil kit. DNA concentration was calculated using a standard curve of known DNA concentrations from *E. coli* K12. 16S qPCR using primers identifying different regions of the V6 16S gene was performed using Kappa SYBR fast mix. Absolute number of bacteria in the samples was then approximated as DNA amount in a sample/DNA molecule mass of bacteria. The same protocol was used to monitor sterility in germ-free mice.

### **Measuring Colonic Epithelial Barrier Permeability by FITC-dextran**

On the day of the assay, 4 kDa fluorescein isothiocyanate (FITC)-dextran was dissolved in phosphate buffered saline (PBS) to a concentration of 80 mg/ml. Mice were fasted for 4 hours prior to gavage with 150 µl dextran. Mice were anesthetized 3 hours following gavage and blood was collected, centrifuged at  $1,000 \times g$  for 12 min at 4°C. Serum was collected and fluorescence was quantified at an

excitation wavelength of 485 nm and emission wavelength of 535 nm.

### **Purification of intestinal epithelial cells for RNA isolation**

Intestinal tissue was excised from mice, thoroughly rinsed with ice-cold PBS to clean the tissue from fecal matter, and opened longitudinally. The tissue was then cut into pieces of 1cm length and incubated in HBSS containing 2mM EDTA and 1mM DTT at 37°C for 30 mins while shaking at 130 rpm. Epithelial cells were collected, filtered, centrifuged, and subsequently stained with anti-EpCAM and anti-CD45 antibodies (Biolegend) for 30 mins on ice. Cells were then washed, resuspended and sorted into lysis/binding buffer (Life Technologies) using a FACS-FUSION cell sorter (BD).

### **RNA isolation and RNA-sequencing**

10<sup>4</sup> cells from each population were sorted into 80 µL of lysis/binding buffer (Life Technologies). mRNA was captured with 12 µL of Dynabeads oligo(dT) (Life Technologies), washed, and eluted at 70°C with 10 µL of 10 mM Tris-Cl (pH 7.5). We used a derivation of MARS-seq as described (51). We sequenced an average of 1 million reads per library (Illumina NextSeq) and aligned them to the mouse reference genome (NCBI 37, mm9) using TopHat v2.0.10 (52) with default parameters. Expression levels were calculated and normalized using ESAT software (<http://garberlab.umassmed.edu/software/esat>). Duplicate reads were filtered if they aligned to the same base and had identical UMIs. Expression levels were calculated and normalized for each sample to the total number of reads using HOMER software (<http://homer.salk.edu>) with the command “analyzeRepeats.pl rna mm9 -d [sample files] -count 3utr -condenseGenes” (53). KEGG analysis was done using DAVID (54).

### **Taxonomic Microbiota Analysis**

Frozen fecal samples were processed for DNA isolation using the MoBio PowerSoil kit according to the manufacturer’s instructions. For the 16S rRNA gene PCR amplification, 1 ng of the purified fecal DNA was used for PCR amplification. Amplicons spanning the variable region V3/4 of the 16S rRNA gene were generated by using the following primers: Fwd 5’-GTGCCAGCMGCCGCGGTAA-3’, Rev 5’-GGACTACHVGGGTWTCTAAT-3’. The reactions were subsequently pooled and cleaned (PCR clean kit, Promega), and the PCR products were then sequenced on an Illumina MiSeq with 500 bp paired-end reads. The reads were then processed using the QIIME analysis pipeline as described (55, 56). In brief, fasta quality files and a mapping file indicating the barcode sequence corresponding to each sample were used as inputs, reads were split by samples according to the barcode, taxonomical classification was performed using the RDP-classifier, and an OTU table was created. Closed-reference OTU mapping was employed using the Greengenes database. Rarefaction was used to exclude samples with insufficient count of reads per sample. Sequences sharing 97% nucleotide sequence identity in the 16S region were binned into operational taxonomic units (97% ID OTUs). For beta-diversity, unweighted UniFrac measurements were plotted according to the two principal coordinates based on 10,000 reads per sample. For microbial distance measurements, unweighted UniFrac distances were compared.

### **Immunofluorescence staining**

Colon samples were extensively washed and fixed and 4% paraformaldehyde. Samples were washed, paraffin-embedded and sectioned. Paraffin sections were de-paraffinized and antigen-retrieved in 10 mM sodium citrate, pH 6. Samples were incubated in PBS containing 20% (v/v) normal horse serum and 0.2% (v/v) Triton X-100 for 1 h; and then incubated over-night with rabbit anti-ZO-1 (Invitrogen 40-2200) primary antibody or rabbit anti E-cadherin (Cell Signaling 24E10). Sections were washed and incubated for 1 hour with alexa 488-conjugated donkey anti Rabbit antibody. Alternatively, sections were stained with Ki67 to indicate proliferating cells.

### **Flow cytometry**

Colonic samples were extensively washed from fecal matter following by 2mM EDTA dissociation at 37°C for 30 mins. Following extensive shaking, the epithelial fraction was used for analysis of EpCAM<sup>+</sup>CD45<sup>-</sup> cells. Colons were then digested using DNAaseI and Collagenase for lamina propria analysis. The isolated cells were washed with cold PBS and resuspended in PBS containing 1% BSA for direct cell surface staining. Single-cell suspensions were stained with antibodies for 30 min on ice against CD3, B220, CD11b, CD45, and CD127. Stained cells were analyzed on a BD-LSRFortessa cytometer and were analyzed with FlowJo software.

For viability measurements, isolated intestinal epithelial cells were stained with EpCAM, CD45 and propidium iodide. Cells were analyzed on a BD-LSRFortessa cytometer. All antibodies were obtained from Biolegend.

### **Ussing chamber**

Epithelial resistance was measured using an Ussing chamber system (Warner Instruments P2300) according to the manufacturer's instructions. In brief, EasyMount chambers were calibrated, colonic tissue was excised from mice and immediately mounted, and voltage clamp recordings were performed. Tissues were maintained at 37°C in physiological salt solution throughout the duration of the recording.

### ***In vitro* barrier assessment**

Caco-2 cells were purchased from ATCC. Cells were routinely grown in regular tissue culture medium (DMEM, 10 % FCS, penicillin/streptomycin, GlutaMAX, 1 g/l glucose). For experiments, cells were seeded onto 96-well glass-bottom plates coated with fibronectin 25 µg/ml 70 000 cells/well and allowed to grow for 48 hours to form confluent monolayer before treatment with indicated concentration of glucose for indicated time period. For immunofluorescent staining cells were permeabilized with 0.5% Triton x100 in 3% paraformaldehyde for 3 minutes and fixed with 3% paraformaldehyde for additional 30 minutes. Tight junctions labeling was performed with primary anti-ZO-1 mouse monoclonal antibodies (BD Transduction Laboratories) 1.25 µg/ml and secondary

Alexa Fluor 488 goat anti-mouse antibodies (Invitrogen) 10 µg/ml. Cells were imaged using DeltaVision wide field fluorescent microscope (GE Healthcare) equipped with 40x/1.3 UPlanFLN objective (Olympus). Cell images were segmented using Morphological Segmentation ImageJ plug-in and junction tortuosity was calculated as a ratio between junction length and Euclidian distance between its ends.

### **Human cohort**

27 healthy volunteers were recruited for blood tests. The following variables were measured from each participant: height, waist circumference, weight, systolic and diastolic blood pressure, heart rate, and hip circumference. Obtained sera were subjected to PRR reporter detection assays (see above). Samples were additionally tested for the following parameters:

HbA1c, red blood cells, mean platelet volume, eosinophils ALT/GPT, lymphocytes, hematocrit, MCHC, hemoglobin, sodium, Red cell distribution width, creatinine, CRP, cholesterol, white blood cells, TSH, phosphorus, monocytes, MCH, HDL cholesterol, platelets, albumin, potassium, AST/GOT, neutrophils, MCV, chloride, basophils, and calcium. Pearson's correlation was used to compute correlations between different parameters.

The study was approved by the local IRB.

### **sCD14 measurements**

Concentrations of sCD14 in the serum were measured using ELISA according to the manufacturer's instructions (DY383, R&D Systems). Briefly, plates were coated over night with capture antibody, incubated with supernatant or serum, washed and incubated with anti-sCD14-biotin antibody and HRP-Avidin before quantification.

### **Statistics**

Data are expressed as mean ± SEM. Comparisons between two groups were performed using Mann-Whitney *U*-test. ANOVA with Tukey's post-hoc test was used for comparison between multiple groups. *K*-means clustering based on Pearson's correlation was used to categorize elements in heatmaps. Survival was assessed by Mantel-Cox (log-rank) test. Linear regression was used to assess correlations between two data sets. *P*-values < 0.05 were considered significant. \* *p*<0.05; \*\* *p*<0.01; \*\*\* *p*<0.001; \*\*\*\* *p*<0.0001.

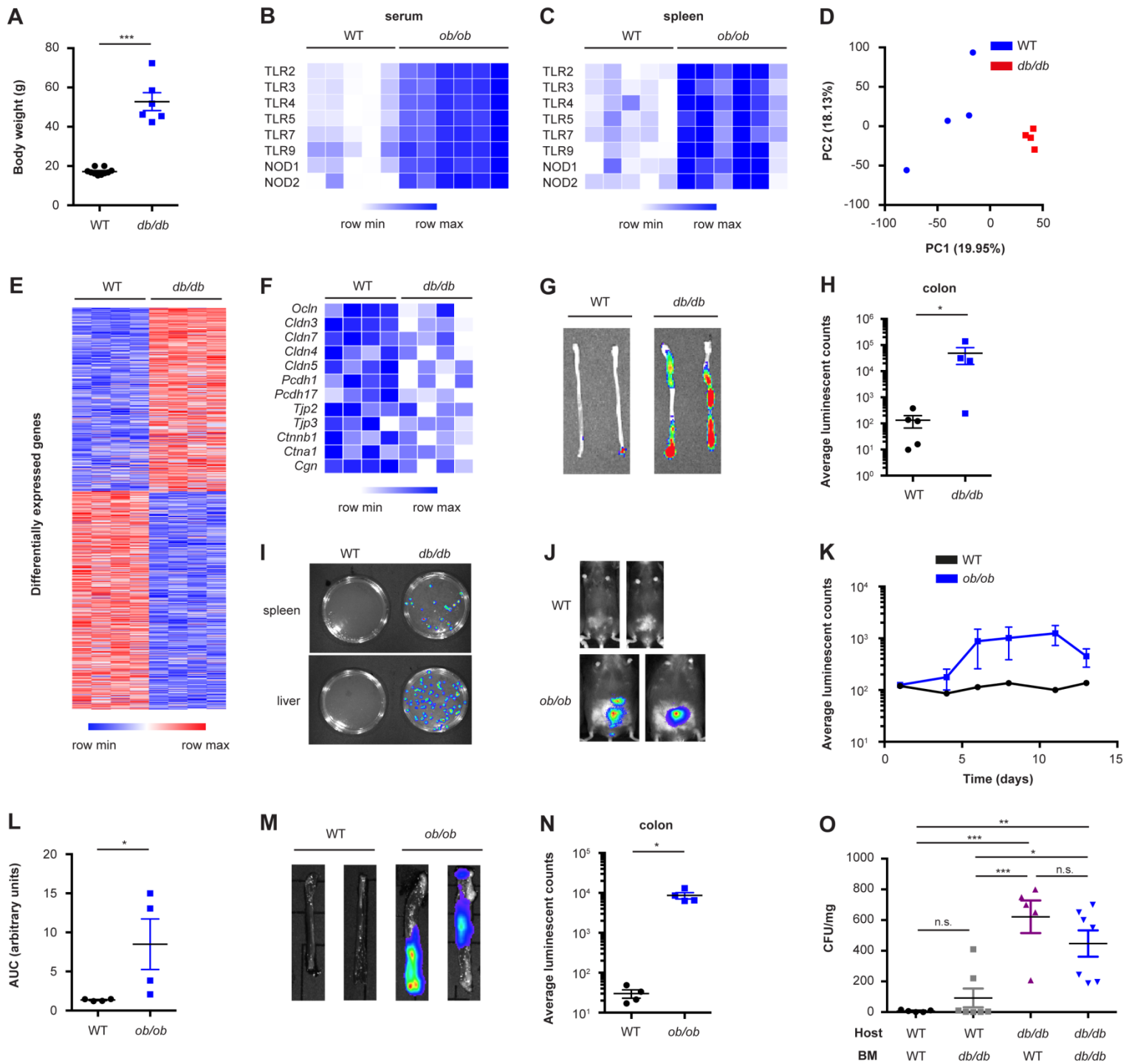


**Fig S1. Obesity predisposes to intestinal barrier dysfunction.** (A) Body weight of 9-week old *db/db* mice and controls. (B, C) PRR stimulation by sera (B) and liver extracts (C) from *db/db* mice. (D) PCA of colonic gene expression in *db/db* mice and WT littermates. (E) Heatmap of differentially expressed genes in the colons of *db/db* mice and WT littermates. (F) Expression of genes related to tight junction formation in the colons of *db/db* mice and WT littermates. (G-N) Representative colonic luminescence (G, M), quantification of colonic luminescence (H, N), representative luminescence from peripheral organs (I), and abdominal luminescence (J, K) from *C. rodentium*-infected *db/db* (G-I) and *ob/ob* mice (J-N). (O) CFUs in mesenteric lymph nodes of *C. rodentium* in bone marrow chimeras of *db/db* and WT mice. Means  $\pm$  SEM are plotted. n.s. not significant, \*  $p < 0.05$ , \*\*  $p < 0.01$ , \*\*\*  $p < 0.001$ , by ANOVA (O) or Mann-Whitney *U*-test (all other panels).

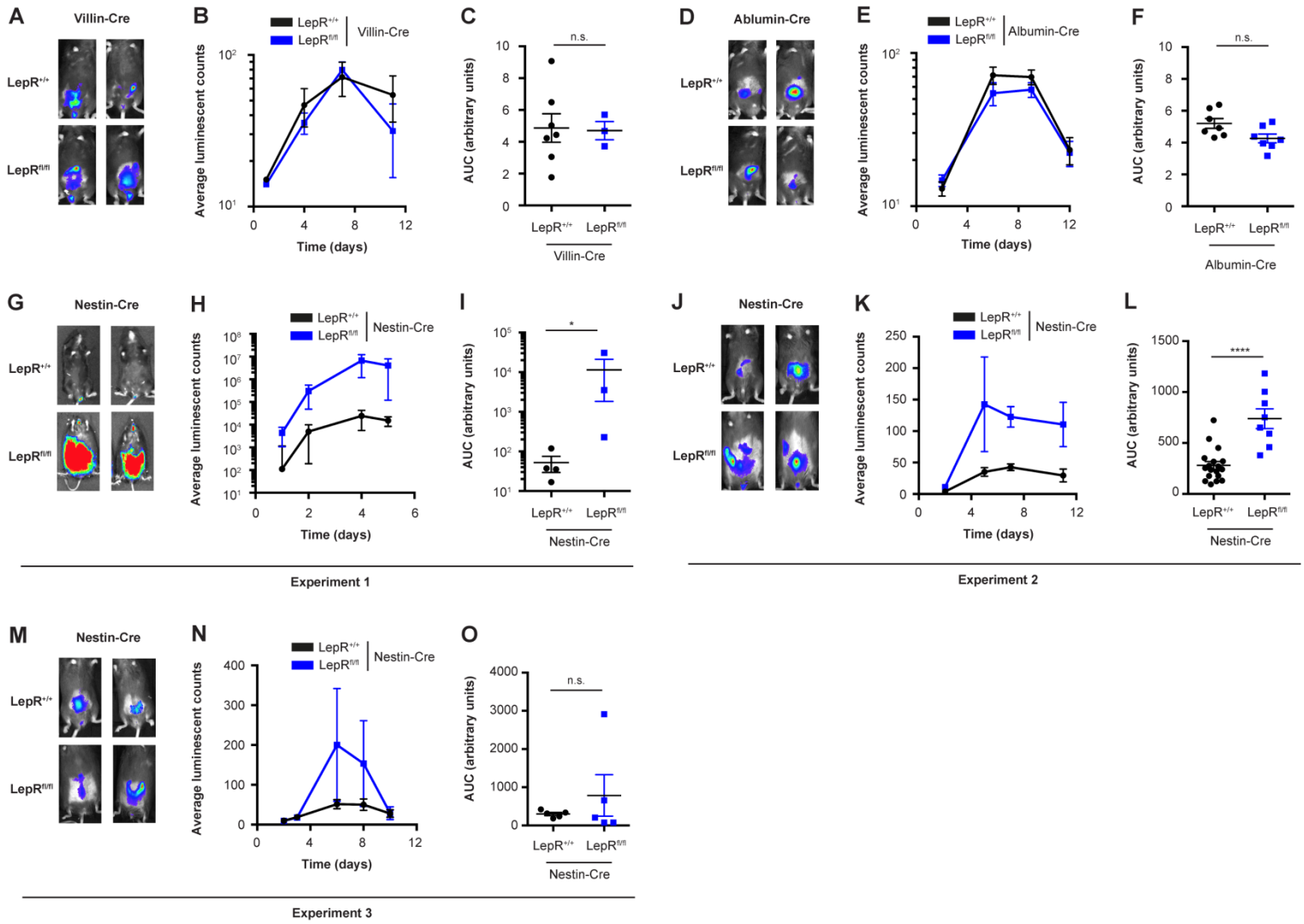


**Fig S2. Analysis of LepR-expressing populations involved in intestinal host defense.** Abdominal luminescence measurements after *C. rodentium* infection of the indicated conditional LepR-deficient mice. The three experiments in G-O were gender- and vivarium-, but not age-matched. Means  $\pm$  SEM are plotted. n.s. not significant, \*  $p < 0.05$ , \*\*\*\*  $p < 0.0001$  by Mann-Whitney *U*-test.

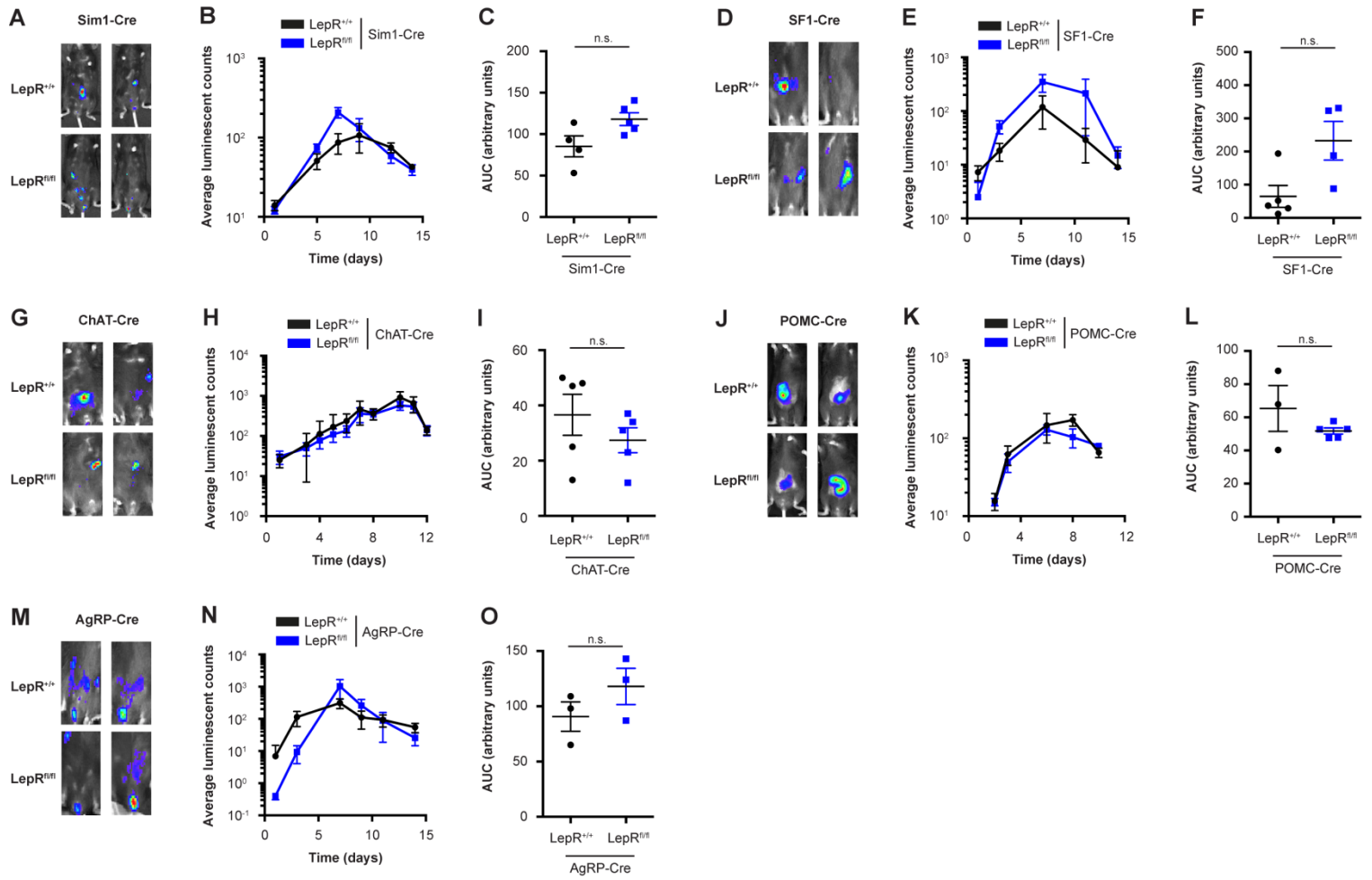


**Fig S3. Analysis of CNS LepR-expressing populations involved in intestinal host defense.** Abdominal luminescence measurements after *C. rodentium* infection of the indicated conditional LepR-deficient mice. n.s. not significant by Mann-Whitney *U*-test.

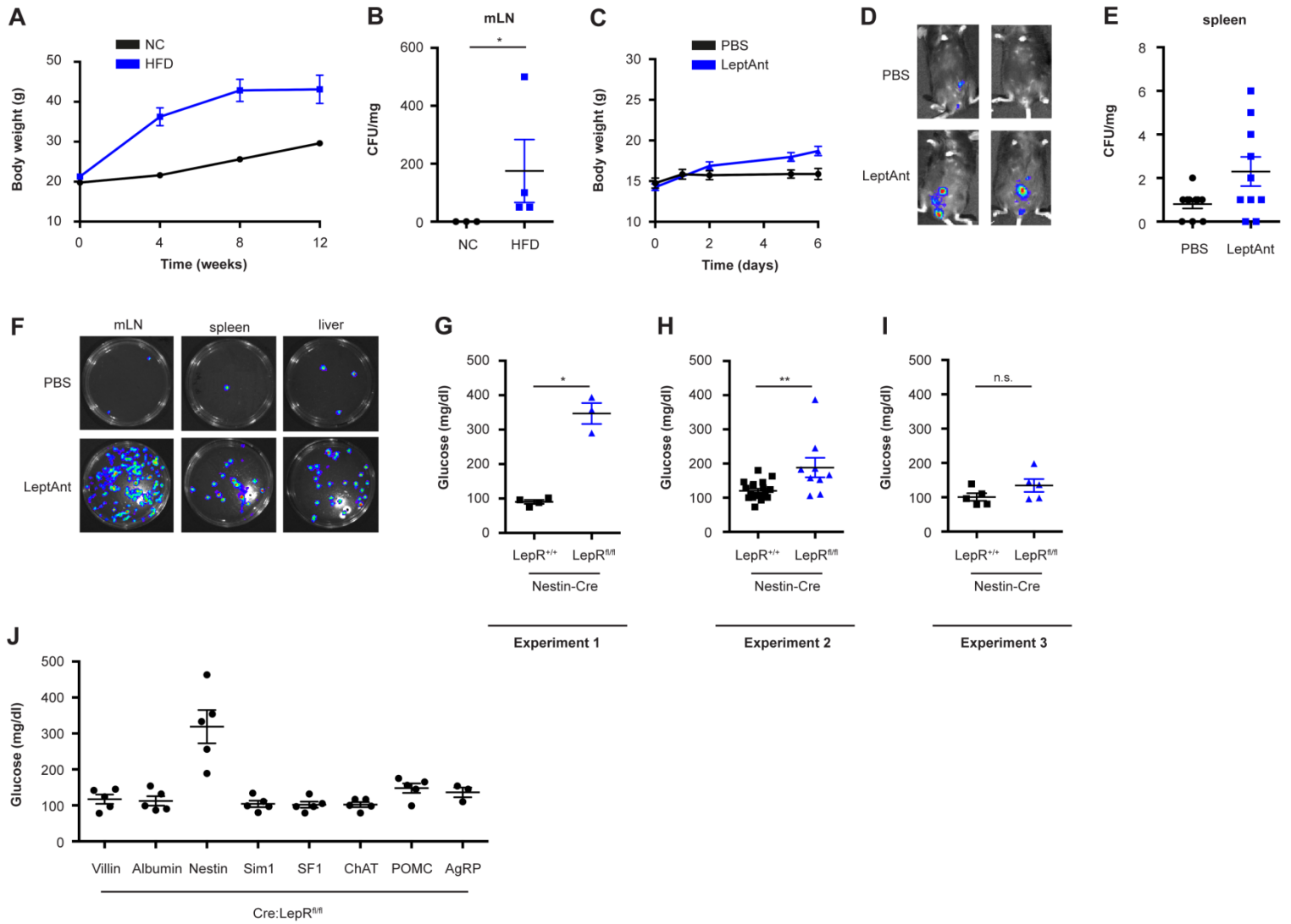


**Fig S4. Obesity *per se* does not explain susceptibility to enteric infection.** (A) Body weight development of mice fed a high-fat diet (HFD). (B) CFUs recovered from mesenteric lymph nodes from HFD-fed mice infected with *C. rodentium*. (C) Body weight development of mice treated with leptin antagonist (LeptAnt). (D-F) Representative abdominal luminescence (D), CFUs recovered from spleens (E) and representative luminescence recordings from internal organs (F) of LeptAnt-treated mice infected with *C. rodentium*. (G-J) Serum glucose levels of the indicated conditional LepR-deficient mice. The three experiments in G-I correspond to fig. S2, G-O. Means  $\pm$  SEM are plotted. n.s. not significant, \*  $p < 0.05$ , \*\*  $p < 0.01$  by Mann-Whitney *U*-test.

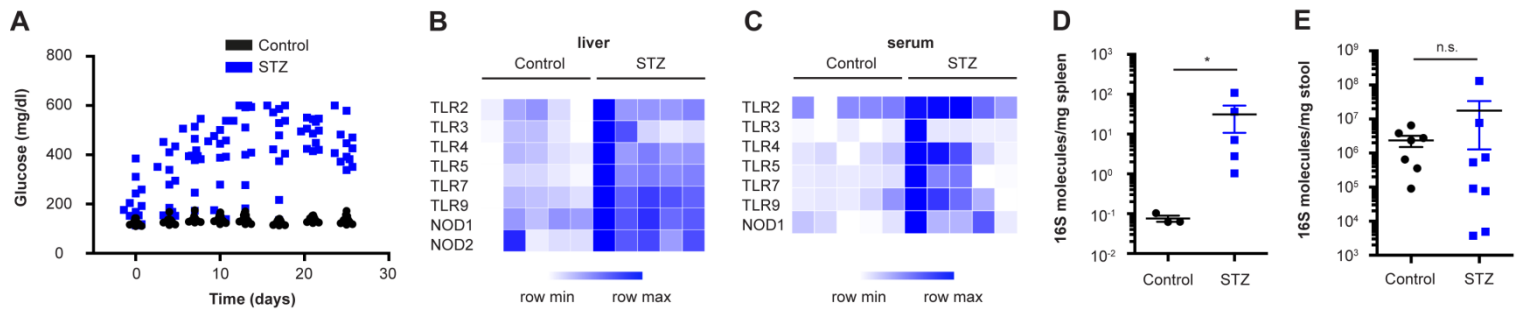


**Fig S5. Hyperglycemia predisposes to intestinal barrier dysfunction.** Serum glucose levels (A), PRR stimulation by livers (B) and sera (C), 16S rDNA quantification in spleens (D) and intestinal lumen (E) from STZ-treated mice and controls. Means  $\pm$  SEM are plotted. n.s. not significant, \*  $p < 0.05$  by Mann-Whitney  $U$ -test.

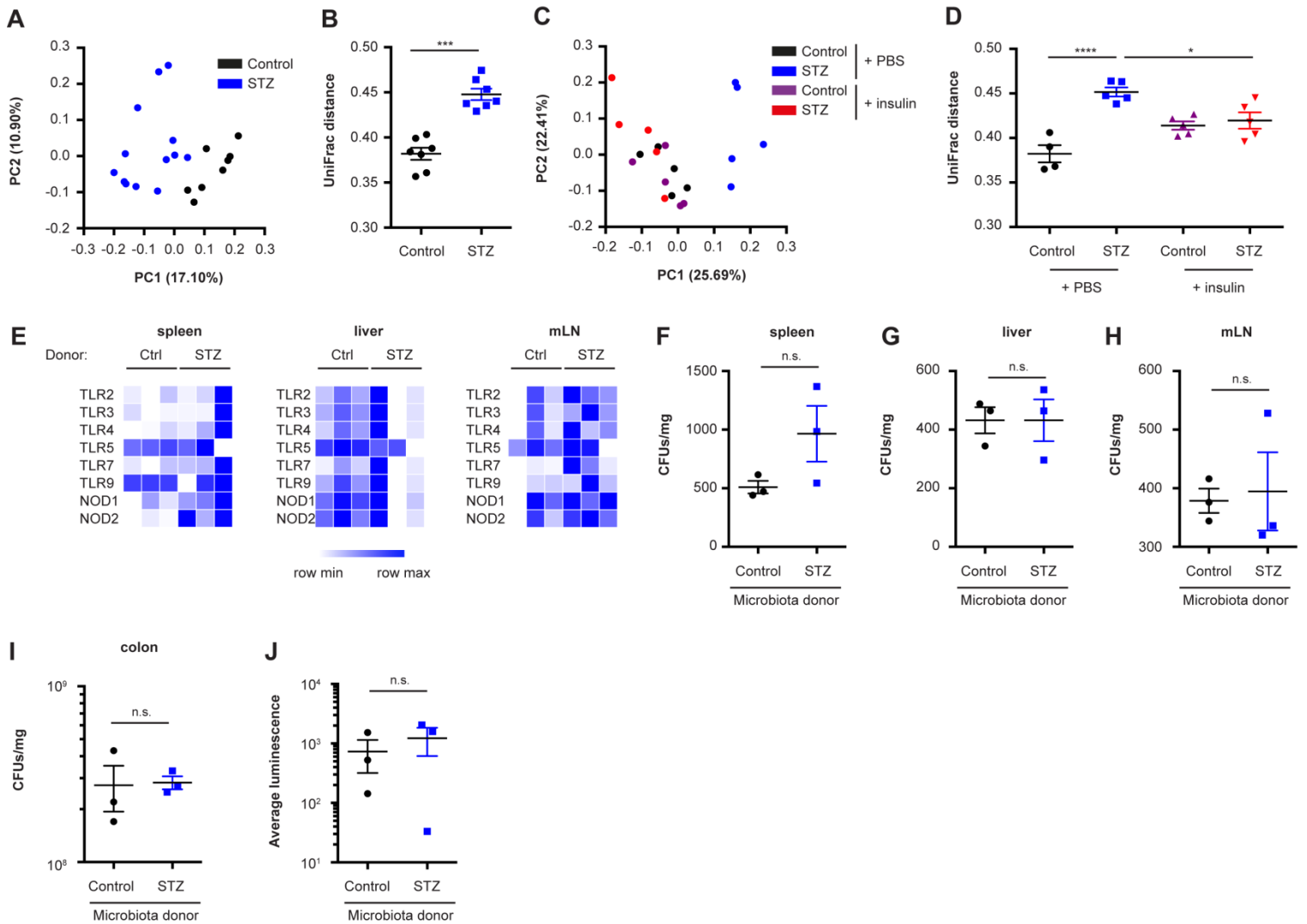


**Fig S6. Dysbiosis does not predispose to intestinal barrier dysfunction.** (A-D) PCoA plots (A, C) and UniFrac distances (B, D) of microbiota samples from STZ-treated mice and controls, with or without additional insulin treatment. (E) PRR stimulation by the indicated tissues from germ-free mice receiving microbiota from either STZ-treated donors or controls. (F-J) Tissue CFUs (F-I) and tissue-adherent colonic luminescence (J) from *C. rodentium*-infected germ-free mice receiving microbiota from either STZ-treated donors or controls. Means  $\pm$  SEM are plotted. n.s. not significant, \*  $p < 0.05$ , \*\*\*  $p < 0.001$ , \*\*\*\*  $p < 0.0001$  by ANOVA (D) or Mann-Whitney *U*-test (all other panels).

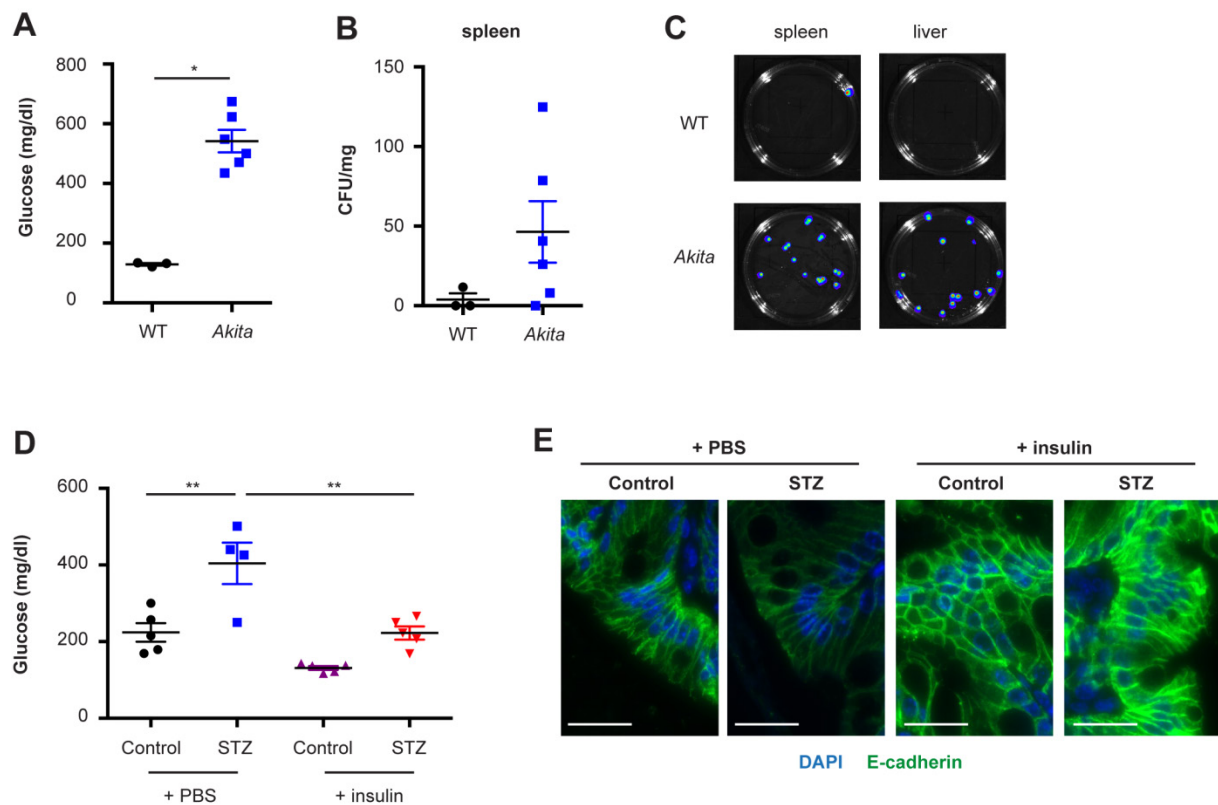


**Fig S7. Additional evidence for hyperglycemia-induced barrier dysfunction.** (A-C) Serum glucose levels (A), splenic CFUs (B) and representative luminescence recorded from spleens and livers (C) of *C. rodentium*-infected *Akita* mice. (D) Serum glucose levels of STZ-treated mice, with or without insulin administration. (E) Representative E-cadherin staining of STZ-treated mice, with or without insulin administration. Scale bars, 25  $\mu$ m. Means  $\pm$  SEM are plotted. \*  $p < 0.05$ , \*\*  $p < 0.01$  by ANOVA (D) or Mann-Whitney *U*-test (A).

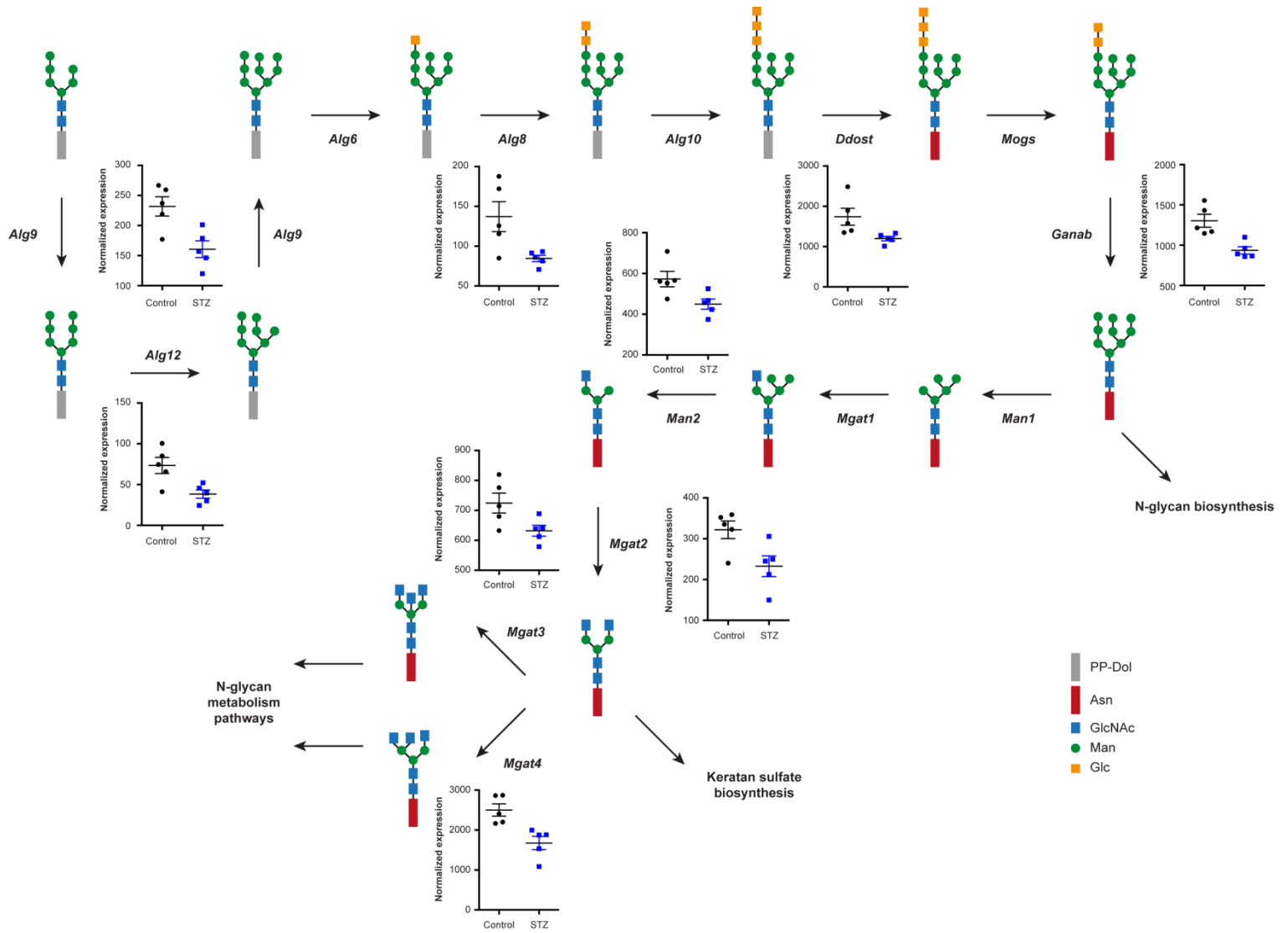


**Fig S8. The impact of hyperglycemia on intestinal epithelial cell function.** RNA-sequencing results obtained from intestinal epithelial cells from STZ-treated mice and controls are shown in a pathway schematic of N-glycan biosynthesis.

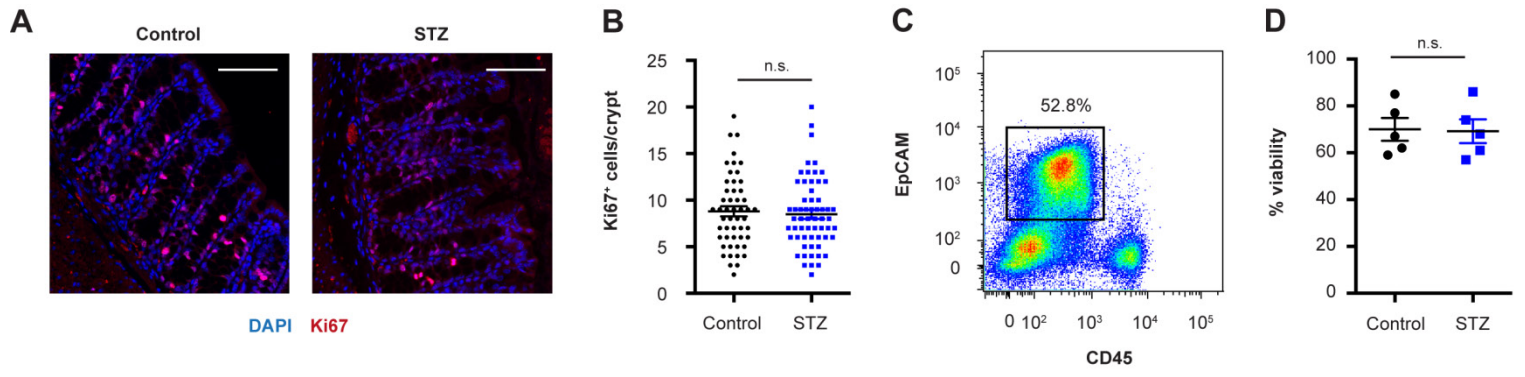


**Fig S9. Hyperglycemia does not alter epithelial turnover.** (A, B) Ki67 staining (A) and quantification (B) of intestinal tissue obtained from STZ-treated mice and controls. Scale bars, 100  $\mu$ m. (C, D) Representative flow cytometry recording (C) and cell viability (D) of intestinal epithelial cells isolated from STZ-treated mice and controls. Means  $\pm$  SEM are plotted. n.s. not significant by Mann-Whitney *U*-test.

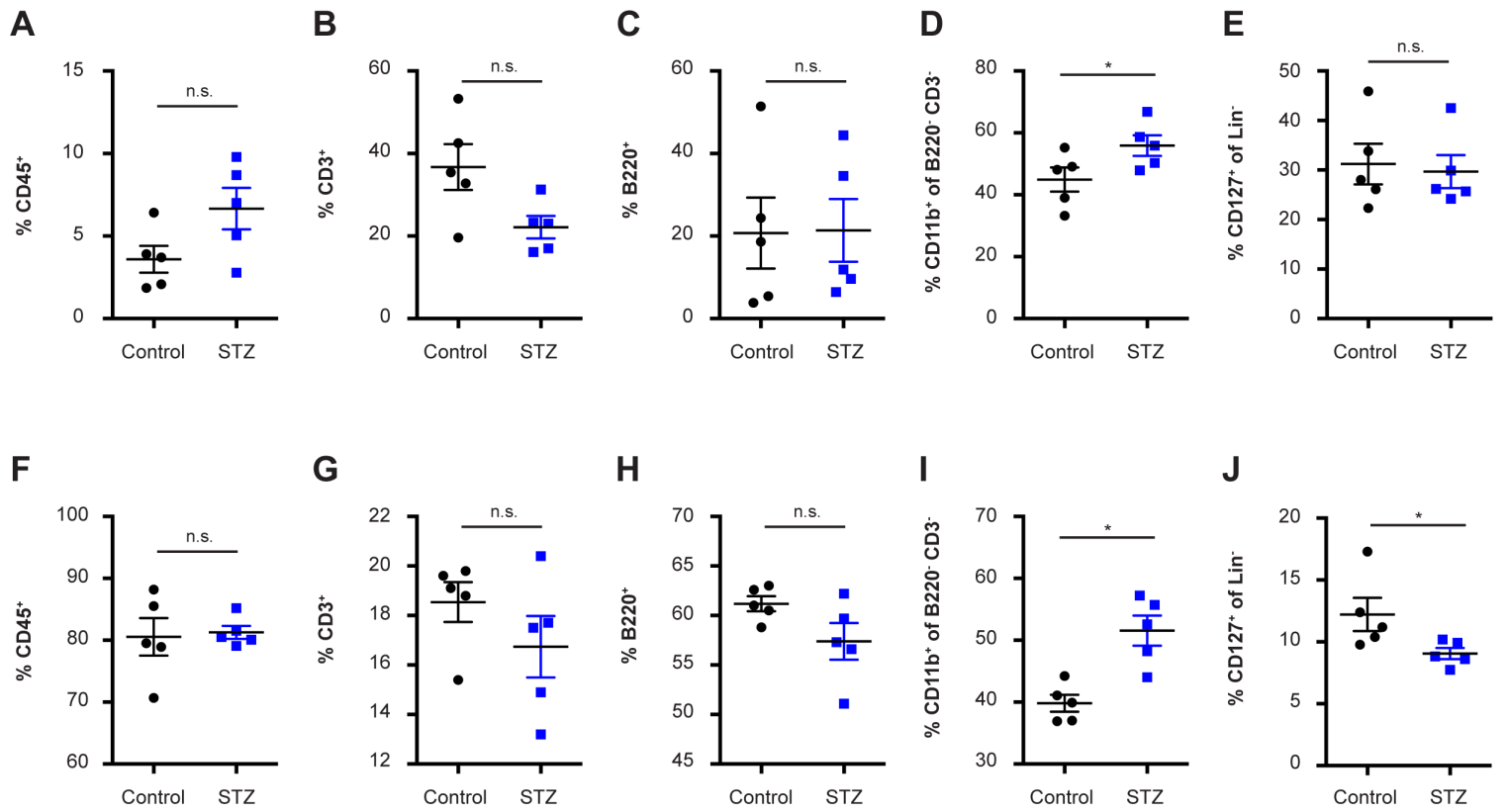


**Fig. S10. The impact of hyperglycemia on immune cell populations.** Relative abundance of the indicated immune cell populations in the colonic lamina propria (A-E) and spleens (F-J) from STZ-treated mice and controls. Means  $\pm$  SEM are plotted. n.s. not significant, \*  $p < 0.05$  by Mann-Whitney *U*-test.

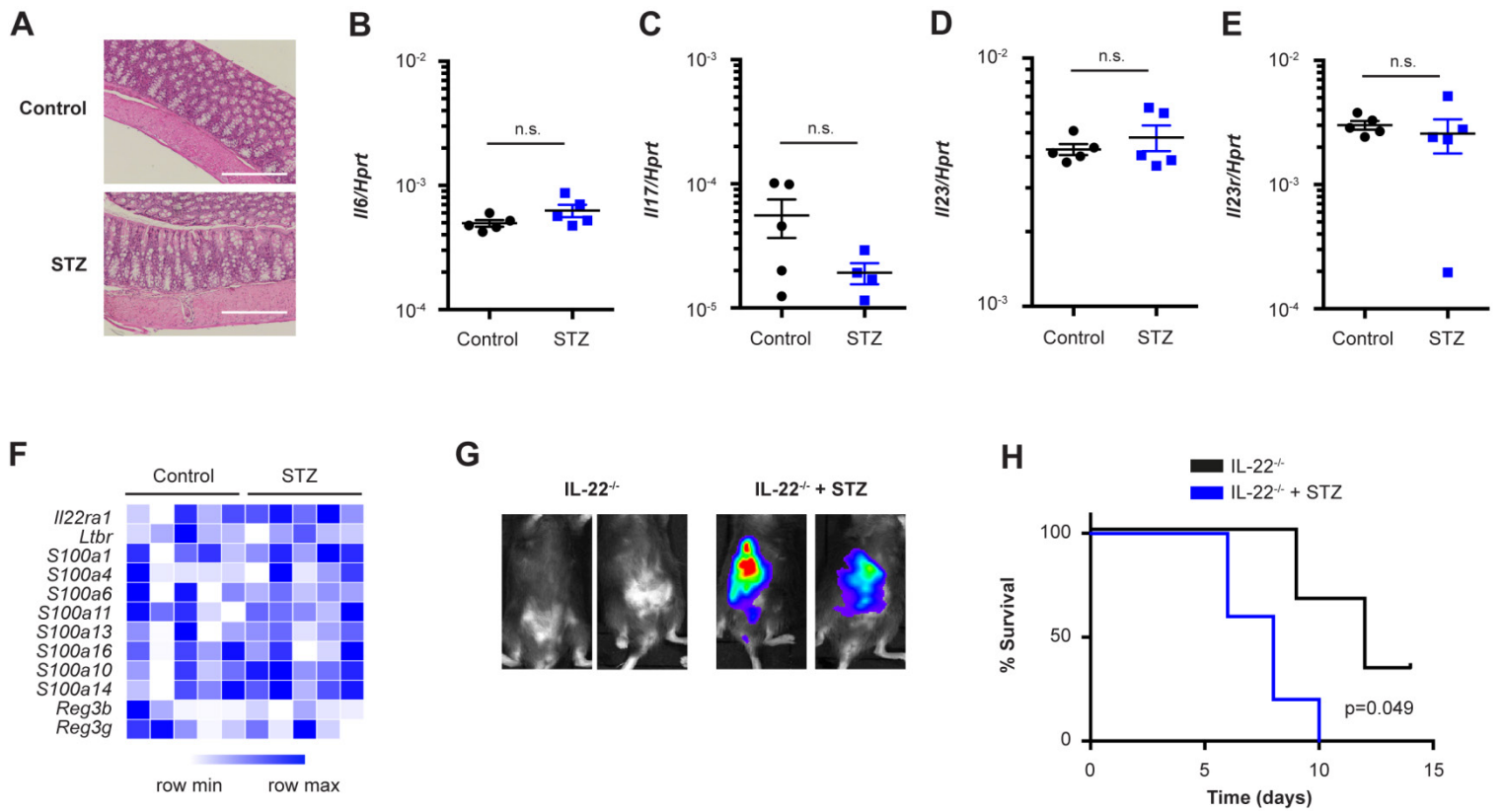


**Fig. S11. The impact of hyperglycemia on IL-22-dependent immunity.** (A) H&E staining of colonic tissue from STZ-treated mice and controls. Scale bars, 200  $\mu$ m. (B-E) Gene expression of the indicated cytokines in colonic tissue from STZ-treated mice and controls. (F) Heatmap of gene expression in intestinal epithelial cells from STZ-treated mice and controls. (G, H) Representative whole body luminescence at early states of infection (G) and mortality (H) of *C. rodentium*-infected STZ-treated *IL-22*-deficient mice and controls. Means  $\pm$  SEM are plotted. n.s. not significant by Mann-Whitney *U*-test.

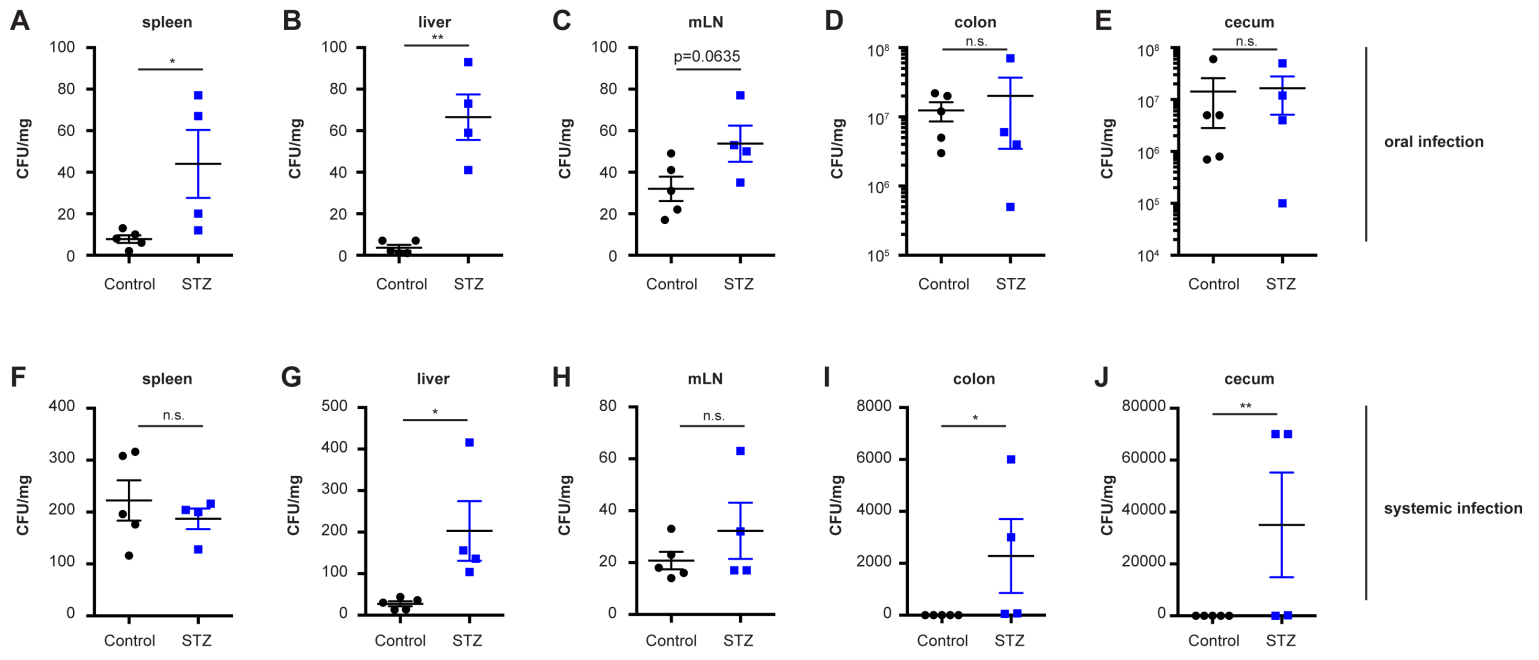


**Fig. S12. Comparison of different infection routes in hyperglycemic mice.** (A-E) CFU of *Salmonella Typhimurium* at the indicated tissues after oral infection. (F-J) CFU of *Salmonella Typhimurium* at the indicated tissues after systemic infection. Means  $\pm$  SEM are plotted. n.s. not significant. \*  $p < 0.05$ , \*\*  $p < 0.01$  by Mann-Whitney *U*-test.

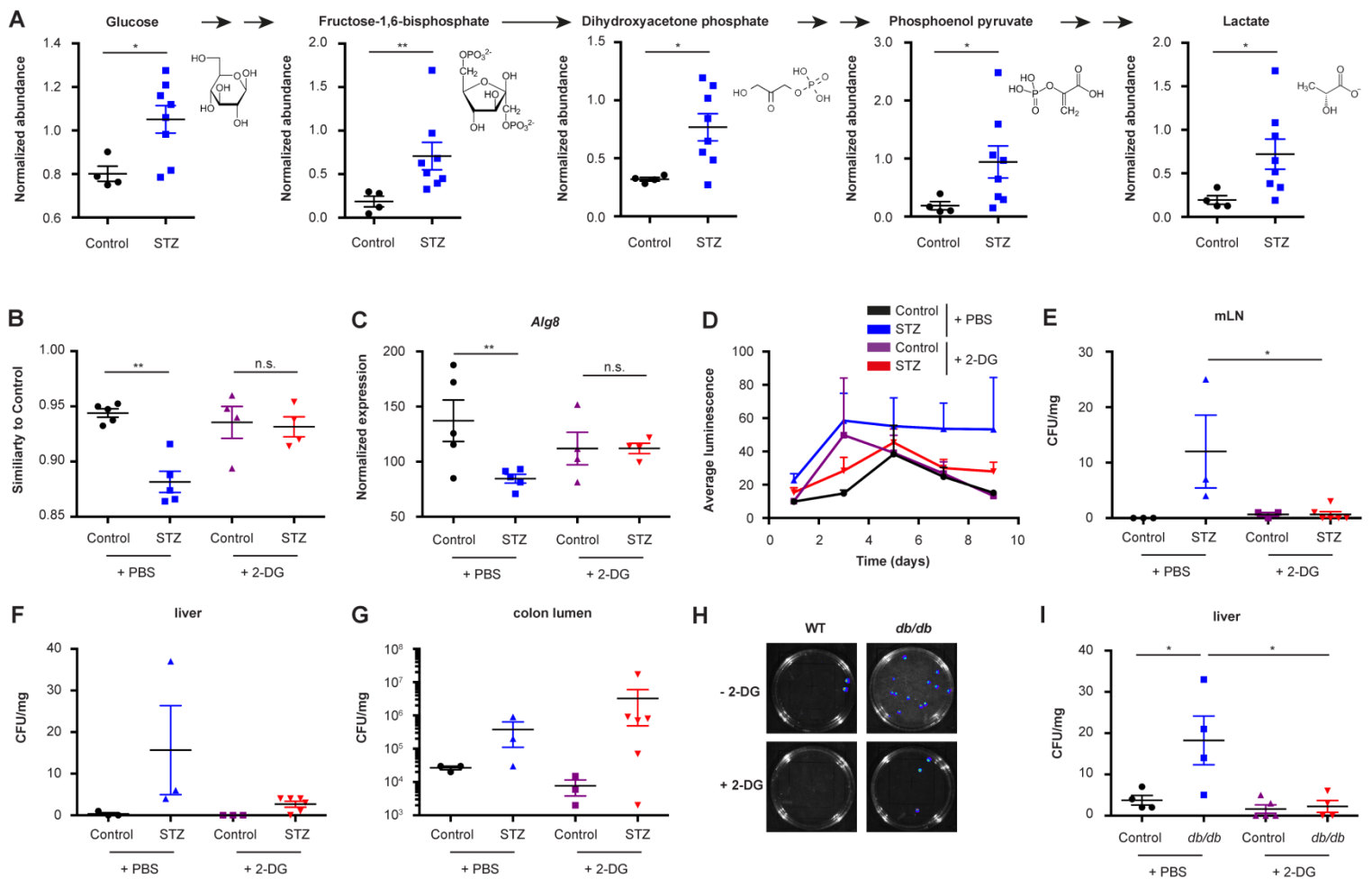


**Fig S13. The impact of 2-deoxyglucose (2-DG) on epithelial function.** (A) Quantification of intestinal epithelial metabolites involved in glycolysis. (B, C) Similarity quantification of the epithelial transcriptome (B) and expression of *Alg8* in colonic epithelial cells (C) from STZ-treated mice and controls, with or without additional 2-DG treatment. (D-G) Abdominal luminescence (D) and bacterial CFUs recovered from the indicated organs (E, F) and from luminal content (G) of STZ-treated *C. rodentium*-infected mice, with or without additional 2-DG treatment. (H, I) Representative luminescence recording (H) and quantification (I) of bacterial CFUs recovered from the livers of *C. rodentium*-infected *db/db* mice, with or without additional 2-DG treatment. Means  $\pm$  SEM are plotted. n.s. not significant. \* p < 0.05, \*\* p < 0.01 by Mann-Whitney *U*-test (A) or ANOVA (all other panels).

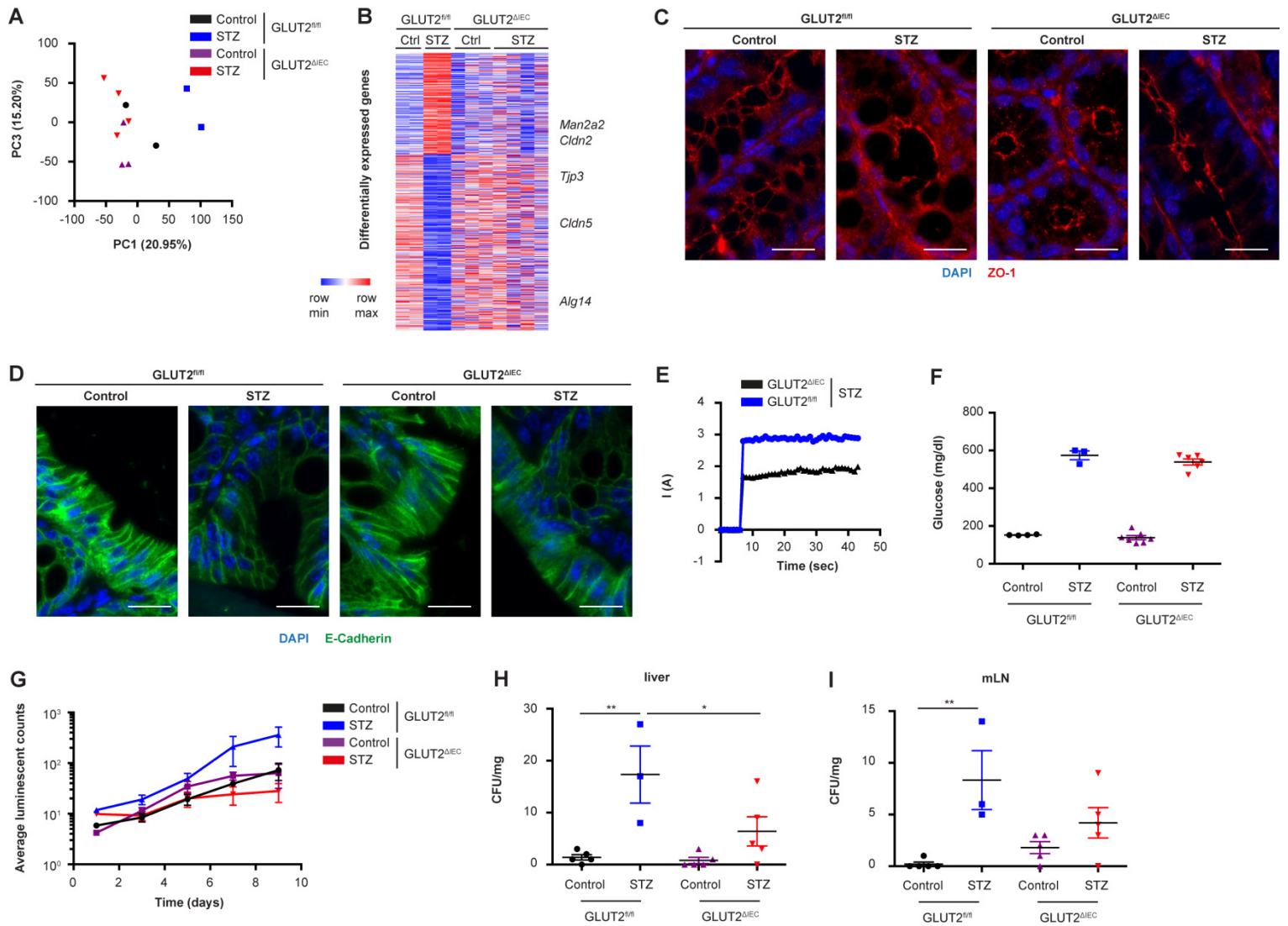


**Fig S14. GLUT2 mediates hyperglycemia-induced epithelial barrier dysfunction.** (A) PCA of epithelial gene expression in STZ-treated GLUT2<sup>ΔIEC</sup> mice and controls. (B) Heatmap of differentially expressed genes in the epithelium of in STZ-treated GLUT2<sup>ΔIEC</sup> mice and controls. (C, D) ZO-1 (C) and E-cadherin staining (D) of colonic tissue from STZ-treated GLUT2<sup>ΔIEC</sup> mice and controls. Scale bars, 25  $\mu$ m. (E) Ussing chamber recording of colonic tissue from STZ-treated GLUT2<sup>ΔIEC</sup> mice and controls. (F) Serum glucose levels in STZ-treated GLUT2<sup>ΔIEC</sup> mice and controls. (G-I) Total body luminescence (G) and CFUs recovered from the liver (H) and mesenteric lymph nodes (H) from *C. rodentium*-infected STZ-treated GLUT2<sup>ΔIEC</sup> mice and controls. Means  $\pm$  SEM are plotted. \*  $p < 0.05$ , \*\*  $p < 0.01$  by ANOVA.

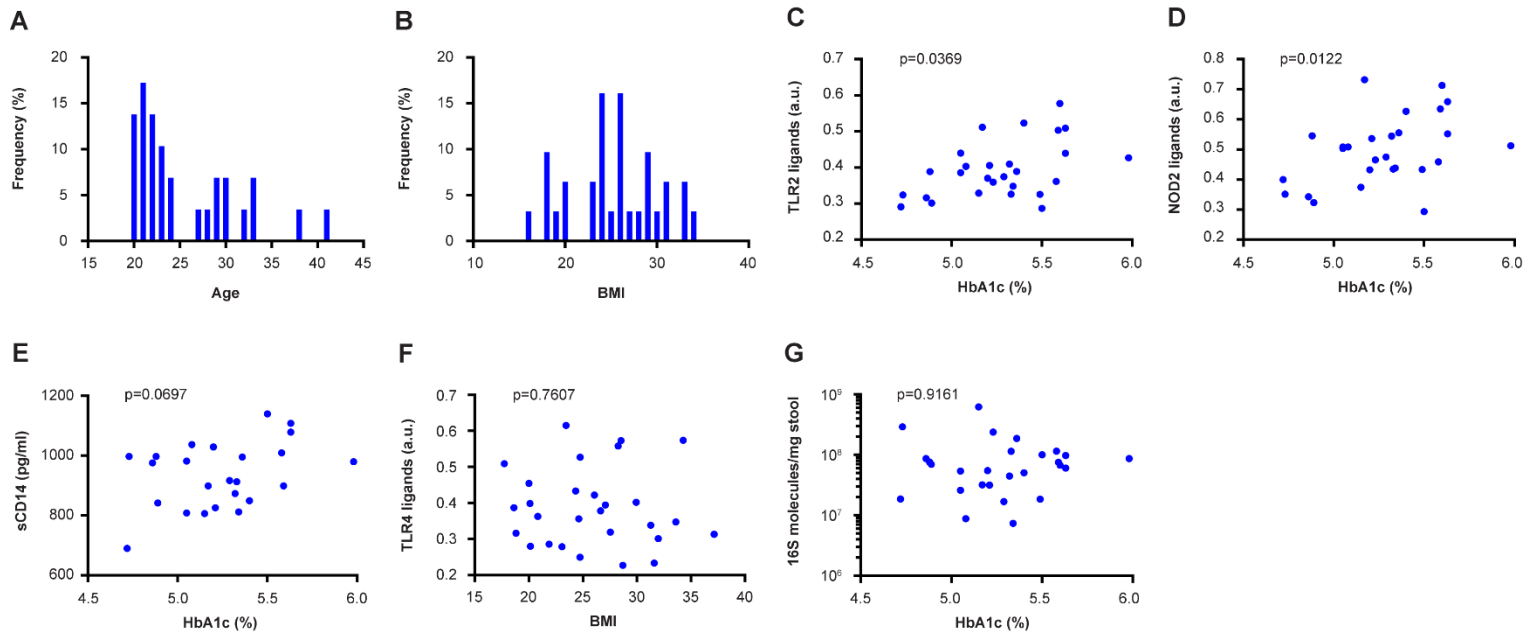


**Fig S15. Correlation between glycemic control levels and influx of microbial products in humans.** (A, B) Age (A) and BMI (B) distribution in the study cohort. (C-G) Correlations between the indicated serum parameters (C-E) and fecal 16S molecules (G) with HbA1c (C-E, G) and BMI (F).

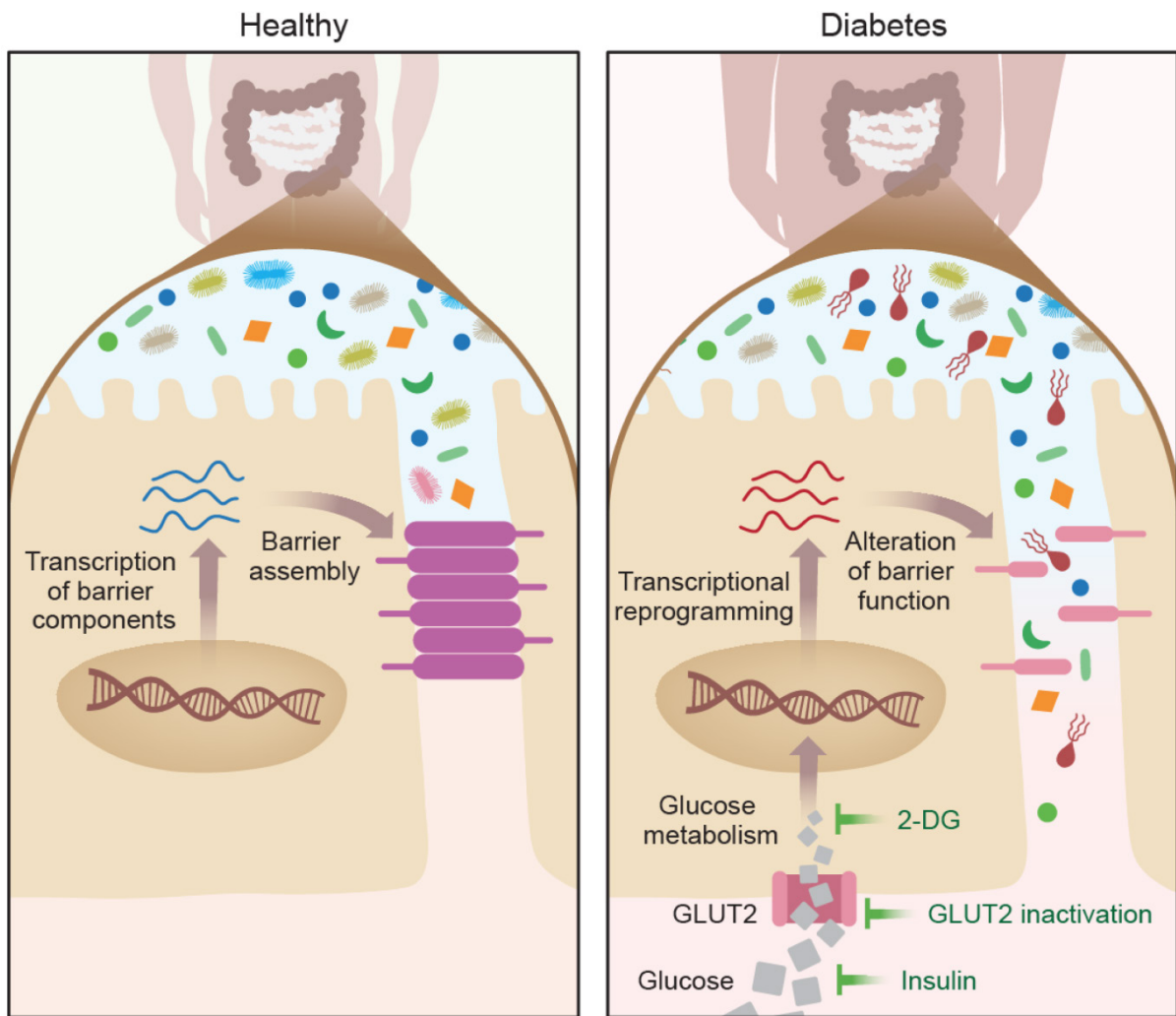


**Fig S16. Schematic of model for hyperglycemia-mediated barrier disruption.**

## References and Notes

1. N. Stefan, F. Schick, H. U. Häring, Causes, characteristics, and consequences of metabolically unhealthy normal weight in humans. *Cell Metab.* **26**, 292–300 (2017). [doi:10.1016/j.cmet.2017.07.008](https://doi.org/10.1016/j.cmet.2017.07.008) [Medline](#)
2. D. A. Winer, H. Luck, S. Tsai, S. Winer, The intestinal immune system in obesity and insulin resistance. *Cell Metab.* **23**, 413–426 (2016). [doi:10.1016/j.cmet.2016.01.003](https://doi.org/10.1016/j.cmet.2016.01.003) [Medline](#)
3. P. D. Cani, R. Bibiloni, C. Knauf, A. Waget, A. M. Neyrinck, N. M. Delzenne, R. Burcelin, Changes in gut microbiota control metabolic endotoxemia-induced inflammation in high-fat diet-induced obesity and diabetes in mice. *Diabetes* **57**, 1470–1481 (2008). [doi:10.2337/db07-1403](https://doi.org/10.2337/db07-1403) [Medline](#)
4. M. E. Falagas, M. Kompoti, Obesity and infection. *Lancet Infect. Dis.* **6**, 438–446 (2006). [doi:10.1016/S1473-3099\(06\)70523-0](https://doi.org/10.1016/S1473-3099(06)70523-0) [Medline](#)
5. K. A. Kaspersen, O. B. Pedersen, M. S. Petersen, H. Hjalgrim, K. Rostgaard, B. K. Møller, C. Juul-Sørensen, S. Kotzé, K. M. Dinh, L. T. Erikstrup, E. Sørensen, L. W. Thørner, K. S. Burgdorf, H. Ullum, C. Erikstrup, Obesity and risk of infection: Results from the Danish Blood Donor Study. *Epidemiology* **26**, 580–589 (2015). [doi:10.1097/EDE.0000000000000301](https://doi.org/10.1097/EDE.0000000000000301) [Medline](#)
6. J. Casqueiro, J. Casqueiro, C. Alves, Infections in patients with diabetes mellitus: A review of pathogenesis. *Indian J. Endocrinol. Metab.* **16** (suppl. S1), 27–36 (2012). [doi:10.4103/2230-8210.94253](https://doi.org/10.4103/2230-8210.94253) [Medline](#)
7. S. I. Grivennikov, K. Wang, D. Mucida, C. A. Stewart, B. Schnabl, D. Jauch, K. Taniguchi, G.-Y. Yu, C. H. Österreicher, K. E. Hung, C. Datz, Y. Feng, E. R. Fearon, M. Oukka, L. Tassarollo, V. Coppola, F. Yarovinsky, H. Cheroutre, L. Eckmann, G. Trinchieri, M. Karin, Adenoma-linked barrier defects and microbial products drive IL-23/IL-17-mediated tumour growth. *Nature* **491**, 254–258 (2012). [doi:10.1038/nature11465](https://doi.org/10.1038/nature11465) [Medline](#)
8. T. R. Sampson, J. W. Debelius, T. Thron, S. Janssen, G. G. Shastri, Z. E. Ilhan, C. Challis, C. E. Schretter, S. Rocha, V. Gradinaru, M.-F. Chesselet, A. Keshavarzian, K. M. Shannon, R. Krajmalnik-Brown, P. Wittung-Stafshede, R. Knight, S. K. Mazmanian, Gut microbiota regulate motor deficits and neuroinflammation in a model of Parkinson's disease. *Cell* **167**, 1469–1480.e12 (2016). [doi:10.1016/j.cell.2016.11.018](https://doi.org/10.1016/j.cell.2016.11.018) [Medline](#)
9. N. Thevaranjan, A. Puchta, C. Schulz, A. Naidoo, J. C. Szamosi, C. P. Verschoor, D. Loukov, L. P. Schenck, J. Jury, K. P. Foley, J. D. Schertzer, M. J. Larché, D. J. Davidson, E. F. Verdú, M. G. Surette, D. M. E. Bowdish, Age-associated microbial dysbiosis promotes intestinal permeability, systemic inflammation, and macrophage dysfunction. *Cell Host Microbe* **21**, 455–466.e4 (2017). [doi:10.1016/j.chom.2017.03.002](https://doi.org/10.1016/j.chom.2017.03.002) [Medline](#)
10. R. Ahmad, B. Rah, D. Bastola, P. Dhawan, A. B. Singh, Obesity-induces organ and tissue specific tight junction restructuring and barrier deregulation by claudin switching. *Sci. Rep.* **7**, 5125 (2017). [doi:10.1038/s41598-017-04989-8](https://doi.org/10.1038/s41598-017-04989-8) [Medline](#)
11. N. M. Mackey-Lawrence, W. A. Petri Jr., Leptin and mucosal immunity. *Mucosal Immunol.* **5**, 472–479 (2012). [doi:10.1038/mi.2012.40](https://doi.org/10.1038/mi.2012.40) [Medline](#)

12. X. Wang, N. Ota, P. Manzanillo, L. Kates, J. Zavala-Solorio, C. Eidenschenk, J. Zhang, J. Lesch, W. P. Lee, J. Ross, L. Diehl, N. van Bruggen, G. Kolumam, W. Ouyang, Interleukin-22 alleviates metabolic disorders and restores mucosal immunity in diabetes. *Nature* **514**, 237–241 (2014). [doi:10.1038/nature13564](https://doi.org/10.1038/nature13564) [Medline](#)
13. R. Madan, X. Guo, C. Naylor, E. L. Buonomo, D. Mackay, Z. Noor, P. Concannon, K. W. Scully, P. Pramoonjago, G. L. Kolling, C. A. Warren, P. Duggal, W. A. Petri Jr., Role of leptin-mediated colonic inflammation in defense against *Clostridium difficile* colitis. *Infect. Immun.* **82**, 341–349 (2014). [doi:10.1128/IAI.00972-13](https://doi.org/10.1128/IAI.00972-13) [Medline](#)
14. C. Guillot, T. Lecuit, Mechanics of epithelial tissue homeostasis and morphogenesis. *Science* **340**, 1185–1189 (2013). [doi:10.1126/science.1235249](https://doi.org/10.1126/science.1235249) [Medline](#)
15. J. W. Collins, K. M. Keeney, V. F. Crepin, V. A. K. Rathinam, K. A. Fitzgerald, B. B. Finlay, G. Frankel, *Citrobacter rodentium*: Infection, inflammation and the microbiota. *Nat. Rev. Microbiol.* **12**, 612–623 (2014). [doi:10.1038/nrmicro3315](https://doi.org/10.1038/nrmicro3315) [Medline](#)
16. M. Wlodarska, C. A. Thaiss, R. Nowarski, J. Henao-Mejia, J.-P. Zhang, E. M. Brown, G. Frankel, M. Levy, M. N. Katz, W. M. Philbrick, E. Elinav, B. B. Finlay, R. A. Flavell, NLRP6 inflammasome orchestrates the colonic host-microbial interface by regulating goblet cell mucus secretion. *Cell* **156**, 1045–1059 (2014). [doi:10.1016/j.cell.2014.01.026](https://doi.org/10.1016/j.cell.2014.01.026) [Medline](#)
17. M. G. Myers Jr., H. Münzberg, G. M. Leininger, R. L. Leshan, The geometry of leptin action in the brain: More complicated than a simple ARC. *Cell Metab.* **9**, 117–123 (2009). [doi:10.1016/j.cmet.2008.12.001](https://doi.org/10.1016/j.cmet.2008.12.001) [Medline](#)
18. E. Elinav, L. Niv-Spector, M. Katz, T. O. Price, M. Ali, M. Yacobovitz, G. Solomon, S. Reicher, J. L. Lynch, Z. Halpern, W. A. Banks, A. Gertler, Pegylated leptin antagonist is a potent orexigenic agent: Preparation and mechanism of activity. *Endocrinology* **150**, 3083–3091 (2009). [doi:10.1210/en.2008-1706](https://doi.org/10.1210/en.2008-1706) [Medline](#)
19. M. S. Islam, D. T. Loots, Experimental rodent models of type 2 diabetes: A review. *Methods Find. Exp. Clin. Pharmacol.* **31**, 249–261 (2009). [doi:10.1358/mf.2009.31.4.1362513](https://doi.org/10.1358/mf.2009.31.4.1362513) [Medline](#)
20. J. Wang, T. Takeuchi, S. Tanaka, S.-K. Kubo, T. Kayo, D. Lu, K. Takata, A. Koizumi, T. Izumi, A mutation in the insulin 2 gene induces diabetes with severe pancreatic beta-cell dysfunction in the Mody mouse. *J. Clin. Invest.* **103**, 27–37 (1999). [doi:10.1172/JCI4431](https://doi.org/10.1172/JCI4431) [Medline](#)
21. D. W. Scott, C. E. Tolbert, D. M. Graham, E. Wittchen, J. E. Bear, K. Burridge, N-glycosylation controls the function of junctional adhesion molecule-A. *Mol. Biol. Cell* **26**, 3205–3214 (2015). [doi:10.1091/mbc.E14-12-1604](https://doi.org/10.1091/mbc.E14-12-1604) [Medline](#)
22. M. Nita-Lazar, I. Rebutini, J. Walker, M. A. Kukuruzinska, Hypoglycosylated E-cadherin promotes the assembly of tight junctions through the recruitment of PP2A to adherens junctions. *Exp. Cell Res.* **316**, 1871–1884 (2010). [doi:10.1016/j.yexcr.2010.02.008](https://doi.org/10.1016/j.yexcr.2010.02.008) [Medline](#)
23. B. T. Jamal, M. Nita-Lazar, Z. Gao, B. Amin, J. Walker, M. A. Kukuruzinska, N-glycosylation status of E-cadherin controls cytoskeletal dynamics through the organization of distinct  $\beta$ -catenin- and  $\gamma$ -catenin-containing AJs. *Cell Health Cytoskelet.* **2009**, 67–80 (2009). [Medline](#)
24. Y. Goto, T. Obata, J. Kunisawa, S. Sato, I. I. Ivanov, A. Lamichhane, N. Takeyama, M. Kamioka, M. Sakamoto, T. Matsuki, H. Setoyama, A. Imaoka, S. Uematsu, S. Akira, S. E. Domino, P. Kulig, B. Becher, J.-C. Renault, C. Sasakawa, Y. Umesaki, Y.

- Benno, H. Kiyono, Innate lymphoid cells regulate intestinal epithelial cell glycosylation. *Science* **345**, 1254009 (2014). [doi:10.1126/science.1254009](https://doi.org/10.1126/science.1254009) [Medline](#)
25. Y. Goto, S. Uematsu, H. Kiyono, Epithelial glycosylation in gut homeostasis and inflammation. *Nat. Immunol.* **17**, 1244–1251 (2016). [doi:10.1038/ni.3587](https://doi.org/10.1038/ni.3587) [Medline](#)
26. T. A. Pham, S. Clare, D. Goulding, J. M. Arasteh, M. D. Stares, H. P. Browne, J. A. Keane, A. J. Page, N. Kumasaka, L. Kane, L. Mottram, K. Harcourt, C. Hale, M. J. Arends, D. J. Gaffney, G. Dougan, T. D. Lawley; Sanger Mouse Genetics Project, Epithelial IL-22RA1-mediated fucosylation promotes intestinal colonization resistance to an opportunistic pathogen. *Cell Host Microbe* **16**, 504–516 (2014). [doi:10.1016/j.chom.2014.08.017](https://doi.org/10.1016/j.chom.2014.08.017) [Medline](#)
27. J. M. Pickard, C. F. Maurice, M. A. Kinnebrew, M. C. Abt, D. Schenten, T. V. Golovkina, S. R. Bogatyrev, R. F. Ismagilov, E. G. Pamer, P. J. Turnbaugh, A. V. Chervonsky, Rapid fucosylation of intestinal epithelium sustains host-commensal symbiosis in sickness. *Nature* **514**, 638–641 (2014). [doi:10.1038/nature13823](https://doi.org/10.1038/nature13823) [Medline](#)
28. K. S. Bergstrom, V. Kissoon-Singh, D. L. Gibson, C. Ma, M. Montero, H. P. Sham, N. Ryz, T. Huang, A. Velcich, B. B. Finlay, K. Chadee, B. A. Vallance, Muc2 protects against lethal infectious colitis by disassociating pathogenic and commensal bacteria from the colonic mucosa. *PLOS Pathog.* **6**, e1000902 (2010). [doi:10.1371/journal.ppat.1000902](https://doi.org/10.1371/journal.ppat.1000902) [Medline](#)
29. M. Van der Sluis, B. A. E. De Koning, A. C. J. M. De Bruijn, A. Velcich, J. P. P. Meijerink, J. B. Van Goudoever, H. A. Büller, J. Dekker, I. Van Seuningen, I. B. Renes, A. W. C. Einerhand, Muc2-deficient mice spontaneously develop colitis, indicating that MUC2 is critical for colonic protection. *Gastroenterology* **131**, 117–129 (2006). [doi:10.1053/j.gastro.2006.04.020](https://doi.org/10.1053/j.gastro.2006.04.020) [Medline](#)
30. S. Niu, Z. Bian, A. Tremblay, Y. Luo, K. Kidder, A. Mansour, K. Zen, Y. Liu, Broad infiltration of macrophages leads to a proinflammatory state in streptozotocin-induced hyperglycemic mice. *J. Immunol.* **197**, 3293–3301 (2016). [doi:10.4049/jimmunol.1502494](https://doi.org/10.4049/jimmunol.1502494) [Medline](#)
31. B. Thorens, GLUT2, glucose sensing and glucose homeostasis. *Diabetologia* **58**, 221–232 (2015). [doi:10.1007/s00125-014-3451-1](https://doi.org/10.1007/s00125-014-3451-1) [Medline](#)
32. C. C. Schmitt, T. Aranas, T. Viel, D. Chateau, M. Le Gall, A.-J. Waligora-Dupriet, C. Melchior, O. Rouxel, N. Kapel, G. Gourcerol, B. Tavitian, A. Lehuen, E. Brot-Laroche, A. Leturque, P. Serradas, A. Grosfeld, Intestinal invalidation of the glucose transporter GLUT2 delays tissue distribution of glucose and reveals an unexpected role in gut homeostasis. *Mol. Metab.* **6**, 61–72 (2016). [doi:10.1016/j.molmet.2016.10.008](https://doi.org/10.1016/j.molmet.2016.10.008) [Medline](#)
33. M. E. Kotas, R. Medzhitov, Homeostasis, inflammation, and disease susceptibility. *Cell* **160**, 816–827 (2015). [doi:10.1016/j.cell.2015.02.010](https://doi.org/10.1016/j.cell.2015.02.010) [Medline](#)
34. A. Bangert, M. Andrassy, A.-M. Müller, M. Bockstahler, A. Fischer, C. H. Volz, C. Leib, S. Göser, S. Korkmaz-Icöz, S. Zittrich, A. Jungmann, F. Lasitschka, G. Pfitzer, O. J. Müller, H. A. Katus, Z. Kaya, Critical role of RAGE and HMGB1 in inflammatory heart disease. *Proc. Natl. Acad. Sci. U.S.A.* **113**, E155–E164 (2016). [doi:10.1073/pnas.1522288113](https://doi.org/10.1073/pnas.1522288113) [Medline](#)
35. Y. Tanaka, P. O. Tran, J. Harmon, R. P. Robertson, A role for glutathione peroxidase in protecting pancreatic beta cells against oxidative stress in a model of glucose toxicity.

- Proc. Natl. Acad. Sci. U.S.A.* **99**, 12363–12368 (2002). [doi:10.1073/pnas.192445199](https://doi.org/10.1073/pnas.192445199) [Medline](#)
36. R. Madonna, R. De Caterina, Cellular and molecular mechanisms of vascular injury in diabetes—part I: Pathways of vascular disease in diabetes. *Vascul. Pharmacol.* **54**, 68–74 (2011). [doi:10.1016/j.vph.2011.03.005](https://doi.org/10.1016/j.vph.2011.03.005) [Medline](#)
37. S. O. Butler, I. F. Btaiche, C. Alaniz, Relationship between hyperglycemia and infection in critically ill patients. *Pharmacotherapy* **25**, 963–976 (2005). [doi:10.1592/phco.2005.25.7.963](https://doi.org/10.1592/phco.2005.25.7.963) [Medline](#)
38. S. A. Leite, S. B. Locatelli, S. P. Niece, A. R. F. Oliveira, D. Tockus, T. Tosin, Impact of hyperglycemia on morbidity and mortality, length of hospitalization and rates of re-hospitalization in a general hospital setting in Brazil. *Diabetol. Metab. Syndr.* **2**, 49 (2010). [doi:10.1186/1758-5996-2-49](https://doi.org/10.1186/1758-5996-2-49) [Medline](#)
39. A. Mor, O. M. Dekkers, J. S. Nielsen, H. Beck-Nielsen, H. T. Sørensen, R. W. Thomsen, Impact of glycemic control on risk of infections in patients with type 2 diabetes: A population-based cohort study. *Am. J. Epidemiol.* **186**, 227–236 (2017). [doi:10.1093/aje/kwx049](https://doi.org/10.1093/aje/kwx049) [Medline](#)
40. L. M. Muller, K. J. Gorter, E. Hak, W. L. Goudzwaard, F. G. Schellevis, A. I. Hoepelman, G. E. Rutten, Increased risk of common infections in patients with type 1 and type 2 diabetes mellitus. *Clin. Infect Dis.* **41**, 281–288 (2005). [doi:10.1086/431587](https://doi.org/10.1086/431587) [Medline](#)
41. R. Medzhitov, Origin and physiological roles of inflammation. *Nature* **454**, 428–435 (2008). [doi:10.1038/nature07201](https://doi.org/10.1038/nature07201) [Medline](#)
42. G. S. Hotamisligil, Inflammation, metaflammation and immunometabolic disorders. *Nature* **542**, 177–185 (2017). [doi:10.1038/nature21363](https://doi.org/10.1038/nature21363) [Medline](#)
43. D. Okin, R. Medzhitov, The effect of sustained inflammation on hepatic mevalonate pathway results in hyperglycemia. *Cell* **165**, 343–356 (2016). [doi:10.1016/j.cell.2016.02.023](https://doi.org/10.1016/j.cell.2016.02.023) [Medline](#)
44. A. Nakamura, M. Yoneda, K. Fujita, K. Tajima, K. Kikuchi, A. Nakajima, S. Maeda, Y. Terauchi, Impact of glucose tolerance on the severity of non-alcoholic steatohepatitis. *J. Diabetes Investig.* **2**, 483–489 (2011). [doi:10.1111/j.2040-1124.2011.00134.x](https://doi.org/10.1111/j.2040-1124.2011.00134.x) [Medline](#)
45. F. Pistrosch, A. Natali, M. Hanefeld, Is hyperglycemia a cardiovascular risk factor? *Diabetes Care* **34** (suppl. 2), S128–S131 (2011). [doi:10.2337/dc11-s207](https://doi.org/10.2337/dc11-s207) [Medline](#)
46. M. Barbagallo, L. J. Dominguez, Type 2 diabetes mellitus and Alzheimer’s disease. *World J. Diabetes* **5**, 889–893 (2014). [doi:10.4239/wjd.v5.i6.889](https://doi.org/10.4239/wjd.v5.i6.889) [Medline](#)
47. A. Wang, S. C. Huen, H. H. Luan, S. Yu, C. Zhang, J.-D. Gallezot, C. J. Booth, R. Medzhitov, Opposing effects of fasting metabolism on tissue tolerance in bacterial and viral inflammation. *Cell* **166**, 1512–1525.e12 (2016). [doi:10.1016/j.cell.2016.07.026](https://doi.org/10.1016/j.cell.2016.07.026) [Medline](#)
48. C. A. Thaiss, S. Itav, D. Rothschild, M. Meijer, M. Levy, C. Moresi, L. Dohnalová, S. Braverman, S. Rozin, S. Malitsky, M. Dori-Bachash, Y. Kuperman, I. Biton, A. Gertler, A. Harmelin, H. Shapiro, Z. Halpern, A. Aharoni, E. Segal, E. Elinav, Persistent microbiome alterations modulate the rate of post-dieting weight regain. *Nature* **540**, 544–551 (2016). [doi:10.1038/nature20796](https://doi.org/10.1038/nature20796) [Medline](#)
49. M. Barthel, S. Hapfelmeier, L. Quintanilla-Martínez, M. Kremer, M. Rohde, M. Hogardt, K. Pfeffer, H. Rüssmann, W.-D. Hardt, Pretreatment of mice with streptomycin

- provides a *Salmonella enterica* serovar Typhimurium colitis model that allows analysis of both pathogen and host. *Infect. Immun.* **71**, 2839–2858 (2003). [doi:10.1128/IAI.71.5.2839-2858.2003](https://doi.org/10.1128/IAI.71.5.2839-2858.2003) [Medline](#)
50. P. K. Anand, R. K. S. Malireddi, J. R. Lukens, P. Vogel, J. Bertin, M. Lamkanfi, T.-D. Kanneganti, NLRP6 negatively regulates innate immunity and host defence against bacterial pathogens. *Nature* **488**, 389–393 (2012). [doi:10.1038/nature11250](https://doi.org/10.1038/nature11250) [Medline](#)
51. D. A. Jaitin, E. Kenigsberg, H. Keren-Shaul, N. Elefant, F. Paul, I. Zaretsky, A. Mildner, N. Cohen, S. Jung, A. Tanay, I. Amit, Massively parallel single-cell RNA-seq for marker-free decomposition of tissues into cell types. *Science* **343**, 776–779 (2014). [doi:10.1126/science.1247651](https://doi.org/10.1126/science.1247651) [Medline](#)
52. C. Trapnell, L. Pachter, S. L. Salzberg, TopHat: Discovering splice junctions with RNA-Seq. *Bioinformatics* **25**, 1105–1111 (2009). [doi:10.1093/bioinformatics/btp120](https://doi.org/10.1093/bioinformatics/btp120) [Medline](#)
53. S. Heinz, C. Benner, N. Spann, E. Bertolino, Y. C. Lin, P. Laslo, J. X. Cheng, C. Murre, H. Singh, C. K. Glass, Simple combinations of lineage-determining transcription factors prime cis-regulatory elements required for macrophage and B cell identities. *Mol. Cell* **38**, 576–589 (2010). [doi:10.1016/j.molcel.2010.05.004](https://doi.org/10.1016/j.molcel.2010.05.004) [Medline](#)
54. G. Dennis Jr., B. T. Sherman, D. A. Hosack, J. Yang, W. Gao, H. C. Lane, R. A. Lempicki, DAVID: Database for Annotation, Visualization, and Integrated Discovery. *Genome Biol.* **4**, P3 (2003). [doi:10.1186/gb-2003-4-5-p3](https://doi.org/10.1186/gb-2003-4-5-p3) [Medline](#)
55. J. G. Caporaso, J. Kuczynski, J. Stombaugh, K. Bittinger, F. D. Bushman, E. K. Costello, N. Fierer, A. G. Peña, J. K. Goodrich, J. I. Gordon, G. A. Huttley, S. T. Kelley, D. Knights, J. E. Koenig, R. E. Ley, C. A. Lozupone, D. McDonald, B. D. Muegge, M. Pirrung, J. Reeder, J. R. Sevinsky, P. J. Turnbaugh, W. A. Walters, J. Widmann, T. Yatsunenko, J. Zaneveld, R. Knight, QIIME allows analysis of high-throughput community sequencing data. *Nat. Methods* **7**, 335–336 (2010). [doi:10.1038/nmeth.f.303](https://doi.org/10.1038/nmeth.f.303) [Medline](#)
56. C. A. Thaiss, M. Levy, T. Korem, L. Dohnalová, H. Shapiro, D. A. Jaitin, E. David, D. R. Winter, M. Gury-BenAri, E. Tatirovsky, T. Tuganbaev, S. Federici, N. Zmora, D. Zeevi, M. Dori-Bachash, M. Pevsner-Fischer, E. Kartvelishvily, A. Brandis, A. Harmelin, O. Shibolet, Z. Halpern, K. Honda, I. Amit, E. Segal, E. Elinav, Microbiota diurnal rhythmicity programs host transcriptome oscillations. *Cell* **167**, 1495–1510.e12 (2016). [doi:10.1016/j.cell.2016.11.003](https://doi.org/10.1016/j.cell.2016.11.003) [Medline](#)